# Development and Sizing of the Mars 2020 Thermal Protection System

Milad Mahzari[1], Robin Beck[1], Helen Hwang[2], Joshua Monk[3], Jonathan Morgan[3]
*NASA Ames Research Center, Moffett Field, CA, 94035, USA*

Joseph Williams[4]
*AMA Inc., Moffett Field, CA, 94035, USA*

Karl Edquist[5]
*NASA Langley Research Center, Hampton, VA, 23666, USA*

**The Mars 2020 entry vehicle successfully delivered the Perseverance rover to the Martian surface on 18 February 2021. The entry vehicle aeroshell was shielded from aerodynamic heating with a thermal protection system (TPS) made of three different ablative materials. This paper provides an overview of the methodology and assumptions employed for the thermal sizing and design of the Mars 2020 aeroshell TPS. The sizing results demonstrate that the as-built thicknesses of the TPS materials were sufficient to withstand the predicted aerothermal environments without exceeding temperature limits of the underlying aeroshell structure. This paper also provides an overview of the ground testing performed in NASA arc jet facilities to verify the performance of flight lot TPS materials. Finally, temperature data returned by thermocouples embedded in the flight vehicle TPS are compared with predictions by the thermal response models used in pre-flight TPS sizing.**

## I. Nomenclature

| | | |
|---|---|---|
| *FOS* | = | factor of safety |
| *conv* | = | convective |
| *q* | = | heat flux |
| *Q* | = | heat load |
| *R* | = | recession |
| *rad* | = | radiative |
| *RSS* | = | root-sum-squared |
| *T* | = | sized thickness |

## II. Introduction

Mars 2020 mission, which launched in July 2020, delivered the Perseverance rover to Jezero crater on Mars to investigate surface geological processes and evaluate habitability and possible life on Mars in the ancient past. During entry and descent in the Martian atmosphere in February 2021, the rover and science instruments were housed in an aeroshell, which was protected against entry environments by the aeroshell Thermal Protection System (TPS). The Mars 2020 aeroshell was intended to be a build-to-print copy of the Mars Science Laboratory (MSL) aeroshell, the previous Mars rover mission that landed in August 2012; therefore, the TPS design was expected to be identical to MSL's and the thicknesses of different TPS components were fixed to MSL design values. This paper will focus on three main topics: 1) the TPS sizing methodology and analysis that was performed to demonstrate that the TPS design had sufficient margin to protect the aeroshell against predicted aerothermal environments, 2) the flight-lot acceptance

[1] Aerospace Engineer, Entry Systems and Vehicle Development Branch, AIAA Member.
[2] Aerospace Engineer, Entry Systems and Technology Division, AIAA Member
[3] Aerospace Engineer, Thermal Protection Materials Branch, AIAA Member.
[4] Aerospace Engineer, Entry Systems and Vehicle Development Branch, AIAA Member.
[5] Aerospace Engineer, Atmospheric Flight and Entry Systems Branch, AIAA Fellow.

testing of the TPS materials in the NASA Ames arcjet complex to verify that the flight-lot materials performed as expected and the thermal response models employed in TPS sizing accurately predicted the material response, and 3) a brief overview of how the temperature data returned by thermocouples installed in the flight TPS compared with the material response model predictions.

Section III provides an overview of the aeroshell geometry and the TPS design. Section IV discusses the TPS sizing and margining process with results. The design trajectory, aerothermal environments, and thermal analysis tools and models are also described in this section. Section V provides an overview of the flight-lot arcjet testing and corresponding thermal analysis. Section VI reviews the comparison of flight temperature data with response model predictions.

## III. Aeroshell and Thermal Protection System Design

The Mars 2020 entry capsule was composed of a 4.5m-diameter, 70-degree sphere-cone forebody with a biconic backshell and a Parachute Closeout Cone (PCC) that covered the parachute system and its support structure. Fig. 1 and Fig. 2 show the Mars 2020 spacecraft and its major subsystems.

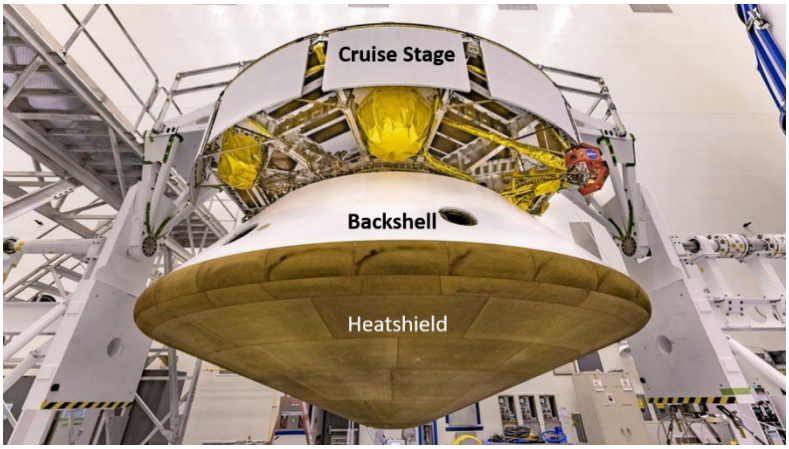


**Fig. 1 Mars 2020 Spacecraft showing different aeroshell subsystems**

The PCC contained a lid through which the parachute was deployed. The Backshell Interface Plate (BIP) was connected to the cruise stage, Parachute Support Structure (PSS), the descent stage and the backshell. The primary function of the BIP and PSS was to anchor these major subsystems and provide the structural load paths necessary to support the launch, entry, parachute mortar fire, and parachute inflation loads. As shown in Fig. 2, the primary TPS materials covering the aeroshell were: Phenolic Impregnated Carbon Ablator (PICA) on the forebody heatshield, Super Lightweight Ablator (SLA-561V) on the backshell and Acusil-II on the BIP, PCC cone, and PCC lid.

### A. Heatshield Design

The heatshield structure was made of an aluminum honeycomb sandwich with graphite fiber facesheets. The facesheet thickness and the aluminum honeycomb core density varied across the heatshield. The nose and flank regions had the lowest number of facesheet plies and lowest density of the honeycomb core. The outer flank and shoulder region, where the heatshield interfaced with the backshell and separation mechanisms, required a thicker facesheet layup and denser core. Denser and thicker substructure provided more thermal mass; therefore, TPS sizing was impacted by this variation in structure. It should be noted that Mars 2020 heatshield structure design is slightly different from MSL design. A structural failure occurred during static testing of a MSL spare heatshield carrier structure, intended to be used for Mars 2020, which motivated a re-design of the structure. A new heatshield was fabricated and design modifications impacted the location on the heatshield that drives TPS sizing as compared to MSL.

The aeroshell structure was shielded from entry aeroheating using a tiled PICA TPS. PICA is made of a carbon fiber preform impregnated with phenolic resin [1]. This material was successfully used on the Stardust and MSL heatshields [2], [3]. PICA tiles were bonded to the structure using HT-424 paste adhesive. The gaps between tiles were filled with Room Temperature Vulcanized (RTV-560) silicone adhesive. The heatshield was sprayed with a silicone coating (NuSil CV-1144-0) to prevent contamination of spacecraft sensors and the clean room environment with phenolic dust that naturally comes off PICA [4].

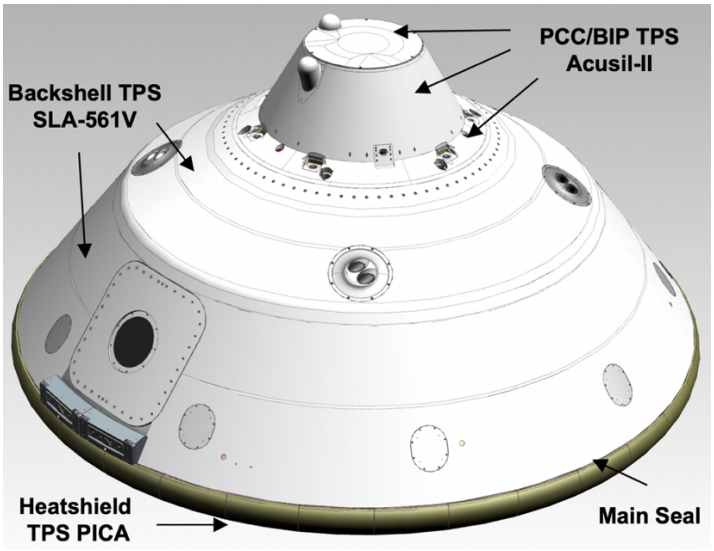


**Fig. 2 TPS materials on Mars 2020 aeroshell**

Fig. 3 shows the PICA tile layout. The entry capsule flew hypersonically at approximately 16 degrees angle of attack, resulting in an off-nose stagnation point. The windward and leeward sides of the heatshield are denoted in this figure. Turbulent transition was predicted to result in higher heating on the leeside tiles. This tile design satisfied multiple aerothermal and manufacturing constraints including PICA billet size, a limit on local fiber orientation with respect to the surface normal, and a limit on the relative angle between tile edges and flow streamlines for a given running length [3]. The nominal PICA thickness was 3.18 cm (1.25 inch) for most of the heatshield, except for the transition tile, the tile between the last flank tile and the shoulder tile, which had a minimum thickness of 3.05 cm (1.20 inch).

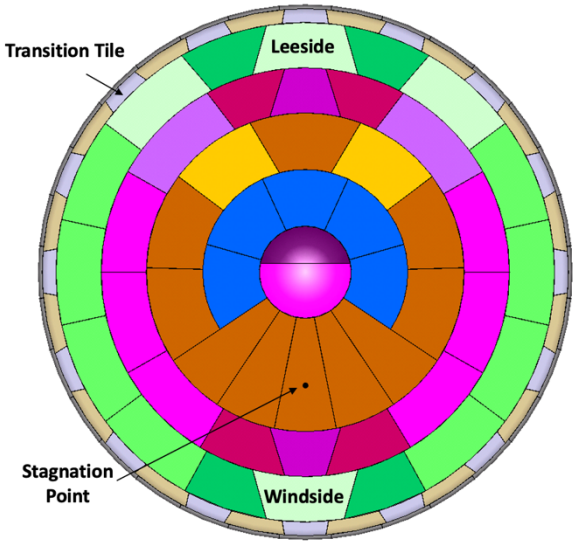


**Fig. 3 Heatshield PICA tile layout**

PICA is an orthotropic material with higher thermal conductivity in-plane than through-the-thickness (TTT). Most of the heatshield tiles were machined out of PICA billets to maintain a small strike angle throughout the tile between the surface normal and the billet TTT direction, with the strike angle being zero at the center of the tile. However, this constraint was not possible for the shoulder tile due to a curved geometry. Therefore, this tile was machined such that the TTT direction is aligned with the surface normal at the inboard edge, where heating is highest, resulting in increasing strike angle (and thus thermal conductivity) toward the outboard shoulder edge. The variations in structure design, PICA thickness and strike angle were all factors in the MSL TPS sizing.

## B. Backshell Design

As shown in Fig. 4, the backshell design contained local features including: Reaction Control System (RCS) thruster cutouts, Multi-Mission Radioisotope Thermoelectric Generator (MMRTG) access door, launchpad access door, separation mechanism covers, a vent and cruise and entry balance mass devices (CMBD and EBMD). These balance masses were deployed prior and during entry to achieve the desired vehicle orientation by shifting the center of mass. While the backshell acreage was covered mostly with SLA-561V, these local features required a variety of thermal protection solutions such as fabric and adhesive seals to shield the backshell against entry environments. The analysis presented in this document focuses only on TPS sizing for the acreage SLA-561V to demonstrate that the as-built thickness was sufficient. The thermal protection design for local features and seals were verified by arcjet or radiant testing and three-dimensional non-ablative thermal analysis.

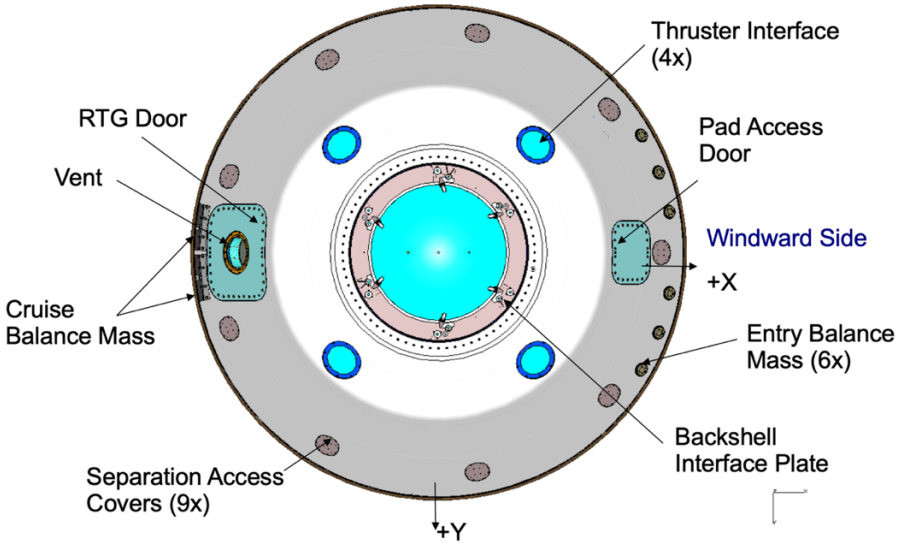


**Fig. 4 Overview of backshell features and interfaces**

SLA-561V is made of RTV silicone resin with granulated cork, silica and phenolic microballoons, and chopped refrasil fibers in a Flexcore honeycomb [5]. This material has been used as either the heatshield or backshell TPS for many Mars and Earth entry missions including Viking, Pathfinder, Mars Exploration Rovers (MER), MSL, Genesis and Stardust. The material was installed on the vehicle first by adhering the Flexcore honeycomb to the backshell structure with HT-424 adhesive followed by hand-packing of the filler material into honeycomb cells. The material was then sprayed with a white paint to achieve desired surface thermal properties during cruise. The nominal uniform thickness of SLA-561V for Mars 2020 was 1.27 cm (0.5 inch), the same as it was for MSL.The backshell structure was made of an aluminum honeycomb sandwich with varying number of graphite facesheet plies. The regions near the BIP and CBMD interfaces were reinforced with higher density cores.

## C. PCC/BIP Design

The TPS material covering the PCC and BIP was Acusil-II, a radio frequency (RF) transparent material that is a mixture of glass fibers, glass microballoons, and silicone. Fig. 5 shows the design details of the BIP, PCC and PCC lid with and without TPS. As can be seen in these diagrams, the hardware was complex and included multiple elements, closeouts, protrusions, and cavities. The PCC was made of a thin aluminum shell that housed the parachute and its support structure. An aluminum doubler was installed at the top of the cone to provide more thermal mass in the high heating windside region, thereby reducing the required TPS thickness (discussed in more detail later). Four Parachute Ultra High Frequency (PUHF) wrap-around antennas were installed on the surface of the cone and provided communication during entry and descent. The Tilted Low Gain Antenna (TLGA) and the Parachute Low Gain Antenna (PLGA) provide additional means of communication. These antennas protruded from the cone and were covered by a radome-shaped structure made of an RF-transparent material called astroquartz. The PLGA radome was part of the PCC lid assembly and the TLGA radome was a separate closeout part that was installed after PCC integration. At the base of the cone, there were six locations (known as blisters) where the cone structure protruded outward to provide clearance to the parachute support structure struts. Cables running to the cruise stage passed through the PCC near the base at 10 and 2 o'clock positions. Cable cutters were installed behind the cone at these two locations to sever the

cables during cruise stage separation. These regions included a closeout structure that was covered by TPS and installed on the PCC. Similarly, a separate closeout was included near the base of the cone at the 6 o'clock position where the PCC mated to the Cruise Medium Gain Antenna (CMGA) on the Cruise Stage. This structure was covered by TPS and installed on the PCC.

Acusil-II was hand-packed on the cone and then machined to the required dimensions. From an aerothermal standpoint, it is highly desirable to maintain a smooth and flush TPS Outer Mold Line (OML); therefore, the local Acusil-II thickness varied depending on the substructure stack. The nominal Acusil-II thickness was 1.74 cm on the aluminum shell; however, in regions where additional elements were attached to the shell, the local thickness was reduced. For example, the Acusil-II thickness was 1.29 cm on the PUHF antennas, 1.50 cm on the windside region covered by the additional aluminum doubler, and 0.26 to 1.64 cm on the blisters. The flushness requirement is also applied to the elements that are subsequently installed on the PCC. For example, the Acusil-II thickness at the base of TLGA was 1.59 cm due to the overlapping of TLGA's astroquartz structure and cone aluminum. Similarly, the cutters had 1.64 cm of Acusil-II due to their additional aluminum structure. The TLGA Radome was covered with 2.50 cm of Acusil-II. All these thicknesses are identical to those flown on MSL.

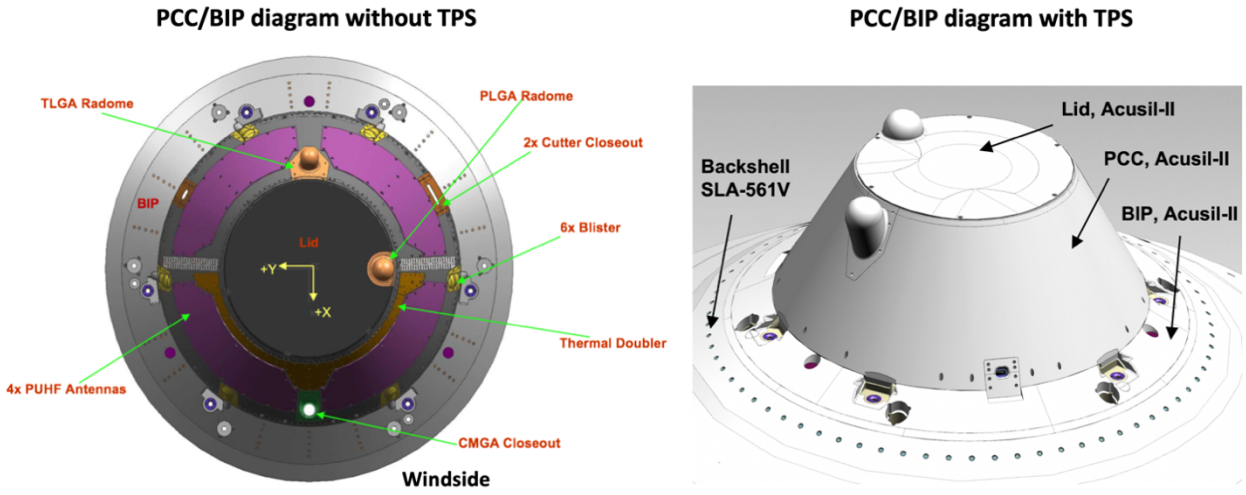


**Fig. 5 PCC/BIP structure and TPS design**

Except for the PLGA radome, which was made of astroquartz and covered with 2.5 cm of Acusil-II, the PCC lid structure was a composite sandwich made of an aluminum honeycomb and graphite facesheets on each side. As shown in Fig. 6b, the structure tapered to only facesheet near the outer edge of the lid. In this region, additional facesheet doublers with varying thicknesses were installed for structural reasons. These variations in the lid structure were important for TPS sizing (discussed in detail later). Acusil-II thickness also varied on the lid. This was done to minimize the lid mass to reduce the risk of recontact after the lid was ejected at parachute deployment. As shown in Fig. 6a, regions where heating was expected to be the highest (windside and leeside edges) had the maximum thickness of Acusil-II while the lid center and the off-center triangular regions on the leeside had minimum thickness of Acusil-II. Cylindrical and linear ramps were used to connect these areas to maintain a smooth OML.

The PCC lid design is mostly based on MSL aerothermal analysis and TPS sizing. In the original MSL design, the maximum Acusil-II thickness was 1.06 cm. For Mars 2020, this was reduced to 0.96 cm to reduce the lid mass after some changes in the parachute pack design required modifications in the lid design that increased its mass.

The BIP interfaced to the cruise stage, PSS, the descent stage and the backshell anchoring all the major Cruise and EDL (CEDL) assemblies together. The structure was made of aluminum, but it was significantly thicker than the PCC due to load carrying requirements. As seen in Fig. 5, the BIP TPS included various cutouts to accommodate six fittings and three pushoff springs that provided the physical interface between the cruise stage and the entry vehicle. Even though these features were not protected by Acusil-II, there was a great amount of structure around them providing significant thermal mass. Their performance was verified by thermal analysis and arcjet testing. They are not within the scope of the TPS sizing study discussed in this paper. The rest of the BIP was fully covered by Acusil-II with thicknesses varying from 2.45 cm near the PCC cone to 4.48 cm at the interface to the backshell, identical to the MSL design.

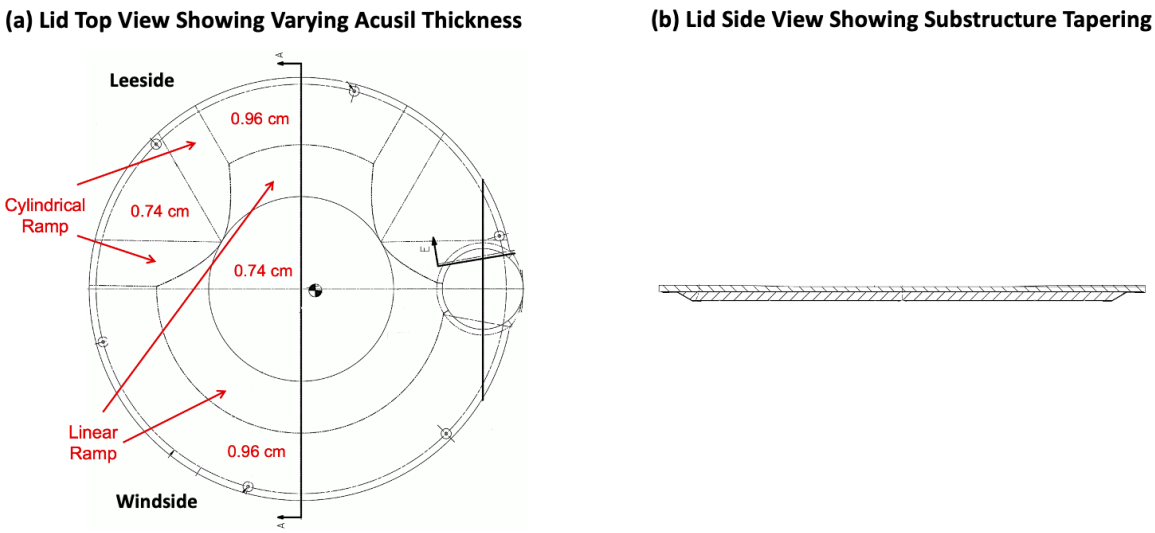


**Fig. 6 PCC lid design and TPS thickness**

## IV. TPS Sizing

### A. TPS Sizing and Margin Process

Conventional NASA sizing of ablating materials relies on a process that accounts for uncertainties in trajectory, aerothermal environments, and material response. Fig. 7 illustrates the sizing process used for Mars 2020 in a simplified diagram. This process is largely derived from the TPS sizing methodology developed by the MSL and Orion teams and was successfully used for those missions [6]. The process starts with choosing an initial nominal trajectory and using aerothermal prediction tools to calculate aeroheating environments. This may be either laminar or turbulent environments, depending on the location on the aeroshell. These simulations are used to derive aerothermal indicators that can be incorporated into trajectory simulation tools to generate quick heating estimates for a given trajectory (discussed in more detail in Section IV-B). A trajectory Monte Carlo study is then performed by considering dispersions in vehicle state and in the atmosphere to identify trajectories that are bounding for TPS thickness. For this study, bounding trajectories were selected as 99%-high in both heat load and heat pulse duration (discussed in more detail in Section VI-B). Aeroheating indicators are then used to generate heating environments for the bounding trajectory at each location selected for TPS sizing.

Next, the material thickness is sized in three branches that account for independent sources of uncertainty. In each branch, the material is sized by determining the thickness that maintains the boundary of the TPS to substructure temperature (the "bondline temperature") below a specified design limit until a time specified by mission designers (typically the time when the hardware has completed its primary function, such as heatshield or backshell release times). The bondline temperature limit is usually based on the performance limits of the adhesive or the substructure. The first branch uses the nominal predicted heating environments and the material is sized to the specified bondline temperature limit. This sizing branch produces an unmargined TPS thickness. In the second branch, a margin factor is applied to the predicted heating environments to account for uncertainties in aerothermal modeling. This margin factor is provided by aerothermal analysts and is typically based on an uncertainty propagation study and/or comparison of model predictions to available ground/flight data. The third branch accounts for uncertainties in material response (modeling and variation in properties). This is typically done by reducing the bondline temperature limit by a bondline temperature margin. This margin is usually derived through a Monte Carlo analysis where input parameters in thermal response modeling (such as thermophysical properties) are varied at a certain sizing location and propagated to bondline temperature dispersions. The thermal margin is typically set to the 3σ dispersion in the maximum bondline temperature (discussed in more detail in Section IV-D). The sized thicknesses from these three branches are combined in a Root-Sum-Squared (RSS) formula, shown in Equation 1.

$$T_{RSS} = T_1 + \sqrt{(T_2 - T_1)^2 + (T_3 - T_1)^2} \tag{1}$$

After the RSS process, a recession margin is added to account for the uncertainties in surface ablation modeling and possible mismatch with ground experiments (needed only for materials that are expected to recede at design

conditions). This process produces the thermally margined thickness, which is then multiplied by a mission-recommended Factor of Safety (FOS) followed by the addition of a manufacturing tolerance to arrive at the final sized thickness for a specific TPS subsystem. This represents the minimum design thickness according to which the TPS must be manufactured.

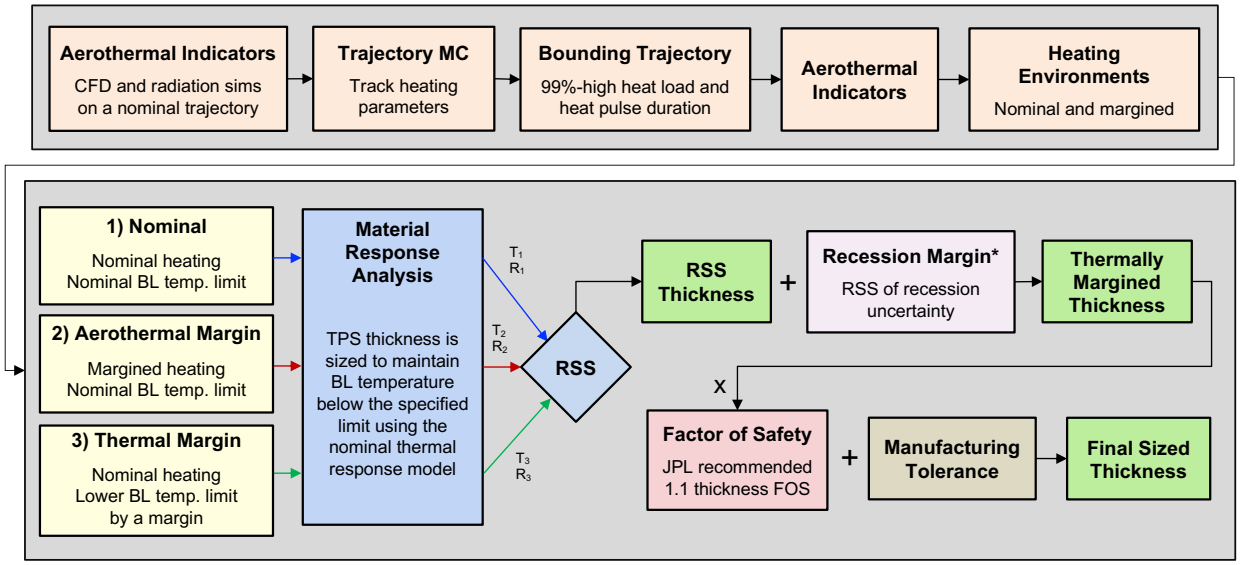


**Fig. 7 Flowchart of the TPS margin process**

As mentioned earlier, TPS thicknesses for Mars 2020 were already pre-determined based on MSL values. Therefore, the goal of this sizing study was not to inform the required TPS thickness for design but to demonstrate that the fixed design thicknesses were sufficient for Mars 2020 environments and conditions. This was done by employing the same process as MSL to size the TPS and then comparing the final sized thickness with the as-built design thickness. In doing so, one could calculate the true FOS in the design thickness according to Equation 2. The design factor of safety expresses the extra thickness available in the design thickness (reduced by manufacturing tolerance) compared to the thermally margined thickness.

$$FOS_{Design} = \frac{T_{Design} - Man.Tol.}{T_{Margined}} \tag{2}$$

Ablative TPS sizing is usually done using one-dimensional (1D) analysis codes at a given location. Typically, the location of maximum heat load determines TPS thickness, assuming uniform TPS across the structure. However, since TPS initial temperature, geometry, and substructure material stack-up vary across the aeroshell, it may not be immediately obvious what combination of these parameters result in the maximum required thickness. In this case, TPS sizing may need to be performed at multiple locations to ensure that the as-built thickness is sufficient at all aeroshell locations. Alternatively, in applications where it is suspected that the as-built TPS is significantly thicker than needed, one can take a conservative approach and perform sizing with a combination of worst-case assumptions (maximum heating, lightest substructure, highest initial temperature, etc.) and show that this worst-case sized thickness is lower than the minimum as-built thickness for a specific TPS component/region. This approach was used for heatshield PICA sizing, where high margins in design thickness were expected, to reduce the amount of analysis needed to show that the heatshield design was sufficient. However, Acusil-II sizing on PCC/BIP was performed at multiple locations due to significant variations in heating and structure configuration combined with suspected lower margins in the design thickness.

It should be also noted that 1D analysis is often acceptable because for the majority of the aeroshell the vehicle configuration is uniform and surface heating varies gradually. However, 1D analysis may be conservative in certain locations where surface heating and structure geometry/configuration vary more abruptly on a smaller scale (such as heatshield shoulder or PCC components). This will be discussed in more detail throughout the document where it is relevant.

The following sections provide more details on the design trajectory, characterization of aeroshell aerothermal environments, and the tools and models used to thermally size Mars 2020 TPS components.

## B. Design Trajectory

MSL aerothermal analysis and TPS sizing was performed for different bounding trajectories throughout the design cycle. These bounding trajectories were identified through Monte Carlo analysis of entry trajectory simulations. The driving trajectory for TPS sizing was selected as the trajectory that produced +3σ heat loads for locations of interest. The final design trajectories for MSL were called 09-TPS-01 (bounding heat load for TPS sizing) and 09-TPS-02 (bounding heat rate) [7], [8]. For Mars 2020, a single design trajectory, named 15-TPS-01, was initially used to complete a preliminary aerothermal analysis and TPS sizing. This trajectory had the highest entry speed within the arrival period for landing locations between +/-30 deg latitude. The analysis performed on this trajectory was used to determine the locations on the aeroshell that drive TPS sizing and to calculate the aerothermal and thermal margins at each sizing location. Later, when entry parameters and vehicle properties were defined more precisely, two additional trajectories were considered for the final design cycle. The main changes compared to 15-TPS-01 were higher vehicle mass, lower entry speed, and an updated atmosphere model. These trajectories were called 19-TPS-01 and 19-TPS-02, representing shallow and steep entry flight path angles. Aeroheating simulations were repeated on these trajectories to derive updated aerothermal indicators [9]. A trajectory Monte Carlo analysis, equipped with updated aerothermal indicators, was performed for each one of these two trajectories to identify how dispersions in vehicle state and entry parameters affect key heating parameters. This analysis helped identify the trajectory from each Monte Carlo set that was deemed bounding for TPS sizing. For each sizing location and trajectory set, the bounding trajectory was identified as the one nearest (and above) 99%-high combined heat load and 99%-high heat pulse duration. Both these parameters were expected to drive TPS sizing based on past experience and preliminary analysis. This selection process is illustrated in Fig. 8 for one sizing location [9].

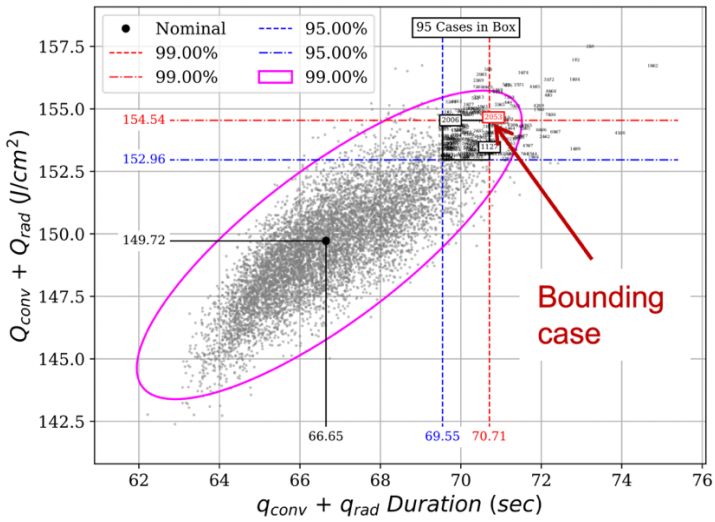


**Fig. 8 Selection of bounding trajectory from the Monte Carlo set at one sizing location**

TPS sizing was performed for the identified bounding trajectory from each Monte Carlo set. The final sized thickness was taken as the larger of two and reported in this document. 15-TPS-01 sizing results were instrumental in identifying sizing locations and thermal margins but are not reported in this paper.

**Table 1 Entry parameters and event times for Mars 2020 design trajectory**

| Trajectory Parameter | 15-TPS-01 | 19-TPS-01 | 19-TPS-02 |
|---|---|---|---|
| Relative Entry Velocity (km/s) | 5.462 | 5.428 | 5.428 |
| Inertial Entry Flight Path Angle (deg) | -15.2 | -15.2 | -15.56 |
| Entry Mass (kg) | 3353 | 3436 | 3436 |
| Parachute Deployment Time, 99%-high (s) | 263 | 259 | 246 |
| Heatshield Separation Time, 99%-high (s) | 285 | 280 | 266 |
| Backshell Separation Time, 99%-high (s) | 428 | 399 | 387 |

Table 1 shows a subset of entry parameters (nominal values) and critical event times for the above-mentioned trajectories. These event times were important for TPS sizing because they set the latest time when bondline temperatures must be maintained below the design limit. Parachute deploy time was used for TPS sizing on the PCC

lid; heatshield separation time was used for PICA sizing; and backshell separation time was used in TPS sizing for backshell, BIP, and PCC cone. As a conservative choice, 99%-high event times were used in TPS analysis (since a Monte Carlo study was not performed for 15-TPS-01, 99%-high event times were estimated based on other similar trajectories).

### C. Aerothermal Environments

For a given trajectory, Computational Fluid Dynamics (CFD) and shock-layer radiation tools are employed to simulate the flow field around the entry capsule at select points in the trajectory. Convective and radiative heat flux estimates can be extracted at locations of interest on the vehicle body. As was the case for MSL, the Mars 2020 aerothermal environments were based on CFD computations using the Langley Aerothermodynamic Upwind Relaxation Algorithm (LAURA) [10], with verification and validation calculations using Data Parallel Line Relaxation (DPLR) [11]. The CFD predictions for Mars 2020 assumed supercatalytic turbulent flow on the forebody, supercatalytic laminar flow on the backshell and non-catalytic laminar flow on BIP/PCC. The main departures of the Mars 2020 analysis from that of MSL were the inclusion of shock layer radiation in the heating environments and the use of non-catalytic convective heating on the Acusil-II surfaces (BIP and PCC). Radiation was neglected for MSL because it was considered insignificant. Analysis and testing since the MSL launch, along with measurements from the Schiaparelli mission [12], have shown that shock layer radiation in the $CO_2$ Mars atmosphere must be included in the heating environment. Radiative heating predictions were based on computations using the High-Temperature Aerothermodynamic Radiation Algorithm (HARA) [13] radiation code, with verification and validation calculations using Nonequilibrium Radiative Transport and Spectra Program (NEQAIR) [14]. The discretized heat flux predictions were curve-fit in time using equations that are functions of trajectory-related parameters like velocity and freestream density. These functions are known as "aerothermal indictors" and were used to provide a time history of heat flux as input environments for material response analysis.

As shown earlier, the TPS margin process accounts for uncertainties in aerothermal calculations by applying margins to the nominal heating environments in the second branch of sizing process. The aerothermal margins account for uncertainties in modeling parameters, code-to-code differences, biases in analysis, and disagreements with ground testing data. Table 2 shows the aerothermal margin factors used for the different capsule regions in Mars 2020 analysis. A detailed description of Mars 2020 entry capsule aerothermal environments and modeling is provided in reference [9].

**Table 2 Aerothermal margin factors for different entry capsule regions**

| Capsule Region / TPS | Convective Heat Flux Margin | Radiative Heat Flux Margin | Surface Pressure |
|---|---|---|---|
| Heatshield / PICA | Varies (1.23*) | 1.41 | Varies (1.24*) |
| Backshell / SLA-561V | 3.0 | 1.47 | 2.0 |
| BIP-PCC / Acusil-II | 3.0 | 1.47 | 2.0 |

* Margin factor for the maximum heat flux location on the heatshield

### D. Thermal Analysis Tools and Models

As was the case for MSL, TPS thermal analysis was performed using the Fully Implicit Ablation and Thermal response (FIAT) program [15],[16]. FIAT performs one-dimensional transient thermal energy transport in a multilayer stack of materials and structure that can ablate from a front surface and decompose in-depth. Version 3.1.2 of FIAT was used for Mars 2020 analysis. This version provides additional features compared to the version used for MSL. PICA sizing used the same thermal response model that was employed in MSL sizing (PICA model v3.3) [17]. This PICA model was developed by Orion Advanced Development Project (ADP) and MSL and is validated against a large set of arcjet test data. A material response model for NuSil coating was not available at the time of this analysis; therefore, the coating was not modeled in PICA thermal analysis. This is a conservative choice since the coating only adds thermal mass to the system. Arcjet testing of NuSil coated PICA samples have shown no degradation in material's performance. Also, the coating is expected to burn off quickly during entry at locations critical for TPS sizing.

SLA-561V sizing was performed using a high-fidelity thermal response model that was developed by NASA in the MSL-era based on extensive material property and arcjet testing data [5]. The white paint on the backshell was not included in the thermal analysis. Again, this is a conservative choice and arcjet tests of SLA samples with the paint showed no degradation in material performance. Acusil-II was sized with the same thermal response model that was used in MSL analysis [18]. All substructure materials were simulated using the same thermal response models used in MSL analysis. The material properties for heatshield and backshell structure were based on extensive thermal

property testing commissioned by Lockheed Martin in support of MSL [19]. Thermal properties for PCC/BIP structure were obtained from testing done by material manufacturers.

PICA thermal analysis used FIAT's full ablative Surface Energy Balance (SEB) option (called "Option 1"). This surface energy balance solved the equilibrium surface chemistry for boundary layer gases, ablation, and pyrolysis products. It also included incoming radiation and surface reradiation terms and accounted for the reduction in convective heating due to the blowing of pyrolysis gases and ablation products (i.e. transpiration cooling). The solution of this surface energy balance yielded recession rate, surface temperature, and conduction into the TPS material which FIAT used as boundary conditions for in-depth heat conduction and decomposition modeling. In Option 1 SEB, convective heat flux is not a direct input and must be expressed in terms of film coefficient and edge enthalpy. These parameters can be readily calculated from CFD-derived convective heat flux indicators and were provided by aerothermal analysts for PICA sizing. Other input parameters include radiative heat flux, surface pressure and blowing parameter as functions of time.

In contrast to PICA, SLA-561V and Acusil-II do not recede at the predicted aftbody heating conditions. Also, application of the film coefficient theory, often utilized for attached forebody flows, is not appropriate in the detached aftbody flow. Therefore, a simpler SEB option in FIAT was used where convective heat flux was input directly (called "Option 3"). Option 3 still included incoming radiation and surface reradiation terms, but did not solve for recession nor account for transpiration cooling from pyrolysis gas blowing, making it a conservative approach. For all TPS materials, an adiabatic surface boundary condition was assumed on the inner mold line of the structure, which is also conservative.

Another important input parameter in thermal analysis and sizing is the TPS initial temperature at entry interface. For all TPS sizing locations presented in this paper, initial temperature predictions are based on cruise and pre-entry thermal modeling done by aeroshell thermal engineers at Lockheed Martin and the NASA Jet Propulsion laboratory (JPL). A 20 ºC margin was added to the predictions to account for variations and uncertainties in modeling.

As shown earlier, the TPS margin process accounts for uncertainties in TPS modeling by applying a bondline temperature margin in the third branch of sizing process. This bondline temperature margin is derived through a Monte Carlo analysis of FIAT simulations where input parameters in thermal response modeling (TPS and substructure thermophysical properties and thicknesses) are varied to determine the resulting dispersion in the bondline temperature. A tool called McFIAT [20] was developed during the MSL-era for this purpose and was also used for the Mars 2020 analysis. Fig. 9 demonstrates in a flow chart the process used to derive the bondline temperature margin. Since the goal of this Monte Carlo analysis is to characterize the dispersions in bondline temperature in a nominal scenario, TPS thickness is set to the unmargined sized thickness at a given location (from the first branch of sizing process). Similarly, nominal unmargined environments are applied. These assumptions produce a dispersed maximum bondline temperature that should have a mean very close to the bondline temperature limit used in sizing. The uncertainties for input parameters are defined either by historical data, statistics gathered from flight-lot material testing, or by expertise. The thermal margin for a specific sizing point is set by subtracting the mean temperature of the cases from this 99.73% percent bounding temperature, representing a 3σ design.

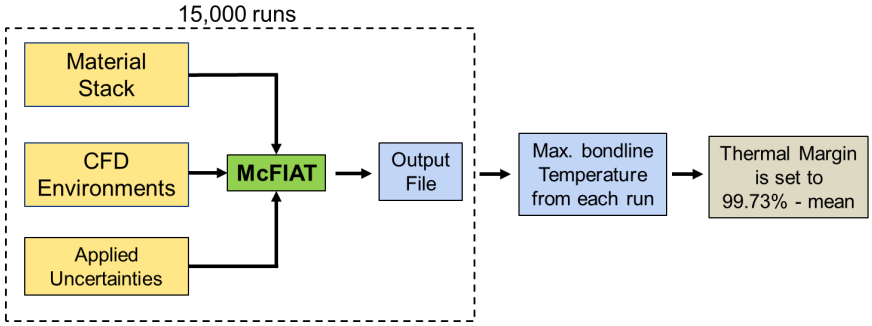


**Fig. 9 Monte Carlo process to derive bondline temperature margin**

### E. Sizing Locations and Results

As mentioned earlier, variations in heating, initial temperature, structure stack-up and TPS design thickness required 1D sizing to be done at many locations to ensure that the design thicknesses were sufficient throughout the vehicle. In regions where it was suspected that the as-built TPS was significantly thicker than needed, such as heatshield and most of backshell, conservative worst-on-worst assumptions were made to reduce the number of sizing

locations that had to be investigated. This allowed the team to focus efforts on more sizing locations on the PCC/BIP where further analysis refinement was required to show that the TPS design thickness had sufficient margins. A total of twenty sizing cases were considered: one on the heatshield, two on the backshell, three on the BIP, eight on the PCC cone and six on the PCC lid. The following sections (1-3) provide the rationale for the selection of sizing locations on the heatshield, backshell and PCC/BIP along with a brief discussion of specific assumptions used in sizing. Section 4 summarizes the final sized thicknesses at all locations and how they compare with as-built thicknesses. Each sizing location is given a name and an environment body point (BP) number which defines its heating environments and its location on an aeroshell map shown in the results section.

*1. Heatshield Sizing Locations and Assumptions*

PICA sizing was performed with a combination of worst-case assumptions with the goal of showing that the minimum PICA design thickness is larger than this worst-case sized thickness. Environments from the maximum heating location (near leeside cone/shoulder tangency point) were applied to the lightest structure stack-up on the heatshield (in the nose region). Additionally, the TPS initial temperature was set to the maximum predicted value for TPS mid-point across the entire heatshield. Heating environments include estimated heating augmentation impact of 0.6 mm surface roughness on turbulent heating. A blowing reduction parameter of 0.3, as defined in [15], was assumed for the turbulent boundary layer. This sizing location was named "Heatshield Max Q" and is labeled as BP2 in the results table shown later in Section IV-E-4.

There were three major differences in the assumptions employed Mars 2020 PICA sizing compared to MSL. The first was the bondline temperature limit. The MSL heatshield went through a post-cure step during its manufacturing process which elevated the entire structure to 250 ºC. Therefore, PICA sizing was done with a bondline temperature limit of 250 ºC based on the logic that the structure had already experienced that temperature prior to undergoing system-level structural testing. The heatshield structure redesign for Mars 2020, motivated by a structure failure during static testing, eliminated this post-cure step to reduce any potential degradation in material strength as a result of elevated temperatures. The structure was cured at 177 ºC; therefore, this value is used as the bondline temperature limit for Mars 2020 sizing.

The second difference was related to a 150% recession lien applied in MSL sizing [6]. MSL and ADP performed many arcjet tests of PICA coupons at different heating conditions in stagnation and shear configurations. Recession measurements from these tests were used to evaluate the accuracy of PICA ablation model. While model predictions agreed well with measurements for stagnation coupons, shear coupon recession measurements were higher than model predictions by an average of ~50% and up to 150% in the worst case. A definitive cause could not be determined at the time; therefore, the project decided to apply a conservative 150% recession lien in PICA sizing as an expedient solution that allowed the team to move forward on an extremely aggressive design schedule without impacting other parallel design activities. Future investigations attributed this recession underprediction to the test coupon holder design where a copper leading edge was resulting in a non-flight-like oxygen-rich boundary layer on the PICA coupon, which was not accounted for in the thermal response analysis. Later tests with graphite leading edges showed better agreement between predictions and measurements. Furthermore, flight data recorded during MSL entry suggest that the thermal response model recession predictions are conservative at MSL flight conditions [21]. Therefore, a recession lien similar to the one used in MSL sizing was not applied for Mars 2020 sizing.

The third difference was the inclusion of shock layer radiation. Radiative heating is not a significant contributor to the total heating on the forebody; however, the inclusion of radiative heating in Mars 2020 environments required an estimate of material absorptivity for thermal analysis. PICA absorptivity measurements were not made extensively during the development of thermal response model because radiative heating was deemed negligible for MSL. Due to lack of reliable data, PICA absorptivity is set to 1.0 (maximum possible value) for Mars 2020 analysis.

*2. Backshell Sizing Locations and Assumptions*

MSL backshell sizing focused mostly on the region closest to the windside heatshield/backshell main seal since the flow is attached on the windside, resulting in the highest convective heating. As mentioned earlier, shock-layer radiation was incorrectly assumed negligible for MSL analysis. The radiative heating can be a significant contributor to the overall heating on the aftbody, especially on the leeside where radiative heating peaks and convective heating is relatively low. Combined with the fact that the initial TPS temperature is considerably higher on the leeside, there was a concern that the leeside seal region may be a driver for TPS sizing. Therefore, the team compared total heat load (convective + radiative) variation on the backshell centerline against the TPS initial temperature variation to determine which locations may be critical for backshell TPS sizing, as shown in Fig. 10. The plot on the left shows the predicted backshell TPS mid-point temperature prior to entry (windside is on the bottom and leeside on the top). The plot on the right side of Fig. 10 shows the total heat load on the backshell centerline (windside is on the left and

leeside on the right side). The team identified four candidate locations for TPS sizing, numbered 1-4 in this figure. Analysis using earlier versions of the entry trajectory showed that the sized thickness for the inner points were much lower than the points at the main seal; therefore, only the seal locations were retained for the final analysis. These two sizing locations were named "Backshell Wind Seal" and "Backshell Lee Seal" and is labeled as BP5 and BP6 in the results table shown later in Section IV-E-4.

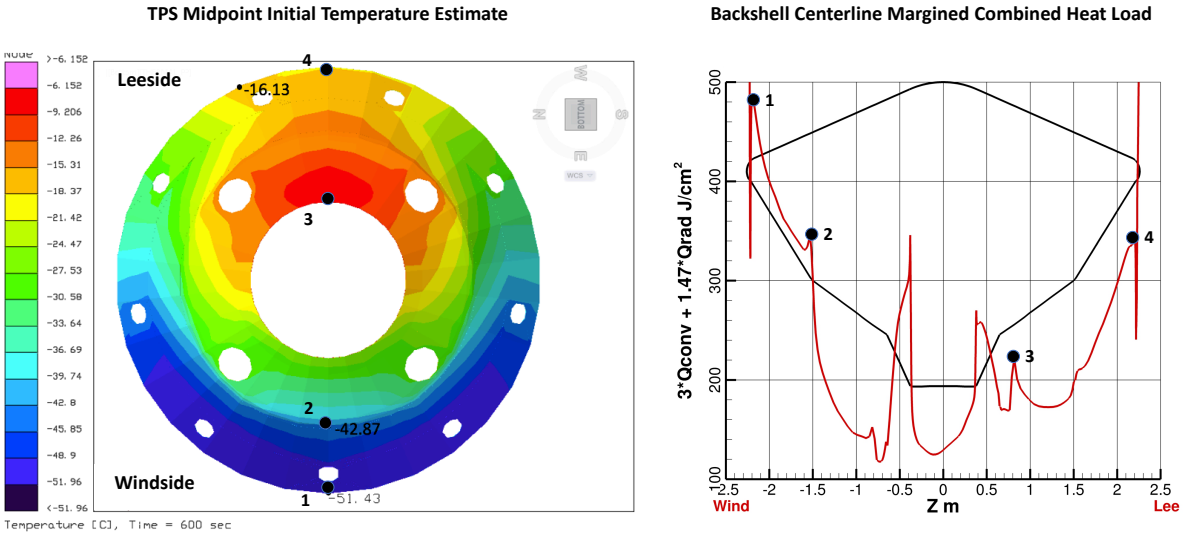


**Fig. 10 Variation in TPS initial temperature and margined heat load on the backshell**

As mentioned earlier, the structure stack-up varies across the backshell. Given that analysis is done at multiple locations, the lightest structure stack-up on the backshell was used in sizing for all body points. This assumption, while conservative, reduces the number of body points that need to be considered and makes the analysis simpler. Similar to PICA sizing, an absorptivity of 1.0 (maximum possible value) is used for SLA-561V due to lack of reliable data.

*3. PCC/BIP Sizing Locations and Assumptions*

As shown earlier, the design of PCC and BIP is quite complex and includes multiple elements, cutouts and protrusions. The material stack and thickness vary from one location to another. Since the underlying structure varies, the maximum allowed temperature at TPS-structure bondline also varies from one location to another. Given that the design thermal analysis tools and material models were one-dimensional, Acusil-II sizing had to be performed at multiple locations with different analysis assumptions to account for the changing substructure, different bondline temperature requirements and varying aerothermal environments.

Fig. 11 shows the convective, radiative and combined heat load contours on PCC/BIP based on Mars 2020 simulations. Convective heating is significantly higher on the windside (bottom) than the leeside (top). The contour map in the middle shows that radiative heating is higher on the leeside and is significantly higher than convective heating in this region. Since radiative heating was neglected for MSL and design TPS thicknesses were based on MSL analysis, more sizing locations on the leeside had to be investigated for Mars 2020 to ensure that the as-built TPS thickness was sufficient. The assumptions and margins applied to aerothermal environments often had to be refined compared to what was used for MSL in an attempt to reduce the sizing environments in the leeside region.

Another aerothermal consideration for BIP/PCC sizing was the transient heating augmentation caused by RCS plume interference. The thrusters are fired intermittently for short periods of time to alter the vehicle bank angle (and lift vector) for entry guidance. Their plume can interact with the aftbody flow field and alter the heating distribution on the backshell. Multiple CFD simulations that included RCS plume were performed as a part of the MSL analysis to understand these effects [8]. The regions on the backshell where there was an increase in the integrated heat load due to RCS firing were identified. This included regions on the BIP and PCC cone that impacted three sizing locations. The environments at these locations were modified by augmenting the nominal heat flux profile up to the maximum heat flux value from MSL RCS-on simulations for a period of eight seconds centered at the peak dynamic pressure time (often the same as peak heat rate time for the aftbody). This was a conservative choice for estimating the worst-case increase in heat load by assuming that RCS firings happen continuously at the peak heating time. The integrated

RCS firing time was estimated to be eight seconds at the most. In reality, RCS firings happen in short periods at times distributed across the trajectory.

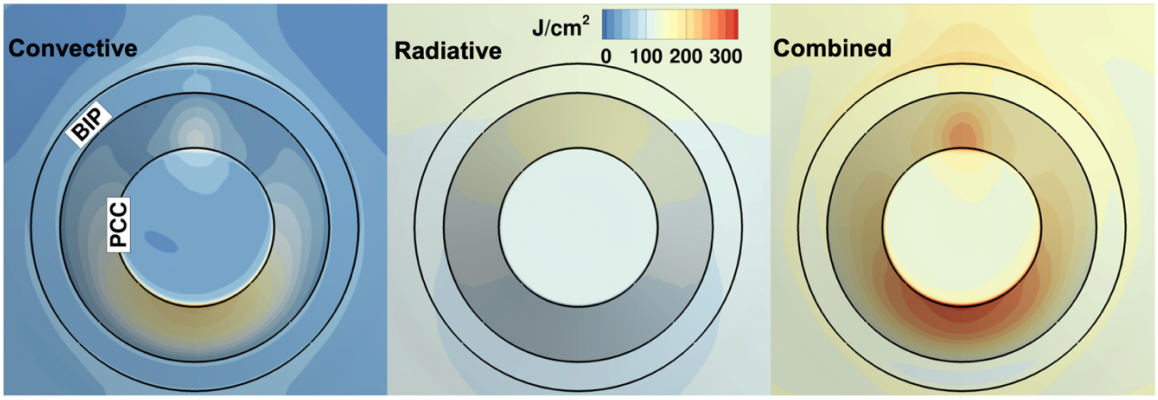


**Fig. 11 Margined convective, radiative, and combined heat load on PCC/BIP**

Three sizing locations were considered on the BIP. Fig. 11 shows that the BIP's leeside experiences the highest combined heat load. Acusil-II thickness on BIP varies from 2.45 cm near the cone to 3.97 cm at the interface to the backshell. Therefore, Acusil-II sizing is done at both the minimum and maximum thickness locations. These two sizing locations were named "BIP Lee PCC" and "BIP Lee BS" and are labeled as BP10 and BP11 in the results table shown in Section IV-E-4. The sizing location at the backshell interface (BIP Lee BS) experiences higher heating but it has the maximum Acusil-II thickness. At the sizing location near the BIP-PCC interface, surface view to the wake flow field is partially obstructed by the PCC cone. This results in a reduction in the total volume available for reradiation. To account for this in TPS sizing, the view factor (percentage of solid angle with view to the wake as opposed to the vehicle surface) was first calculated from the CFD grid. This view factor was then used to decrease the Acusil-II emissivity in the FIAT material response by the same ratio. Decreasing the emissivity by this ratio is analogous to decreasing the solid angle available to this body point to reradiate as a part of the FIAT energy balance. This decrease corresponds to a reduction of 17.5% in emissivity. Additionally, a third sizing location was considered on the right side of the BIP (at 3 o'clock) where MSL RCS-on simulations showed local heating augmentation at the interface between the BIP and the backshell. The smooth-OML heat flux profile was augmented for this location as described earlier. This sizing location was named "BIP Side RCS" and labeled as BP12.

Five unique sizing locations were considered on the PCC cone. Fig. 12 shows the location of these sizing cases overlaid on the PCC structure diagram. A description of each sizing case and rationale for including them in this study is presented below.

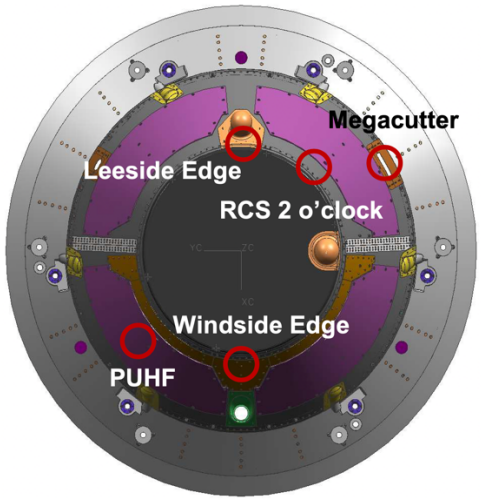


**Fig. 12 PCC cone sizing locations overlaid on the structure diagram**

Windside Edge (BP13): This is the location of maximum heat load on the PCC cone. However, an aluminum doubler is installed in this region to provide additional thermal mass. The doubler leads to reduced TPS thickness at this location. This location is considered due its reduced Acusil-II thickness and unique structure stack.

PUHF Antenna (BP13): There are four PUHF Antennas installed on the cone resulting in reduced TPS thickness and increased thermal mass. As a conservative choice, sizing for this region is done using the windside edge environments which bound environments experienced by the PUHF antennas (the windside antennas extend very close to the top edge of the PCC).

Leeside Edge (BP14): Regions without PUHF antenna or doubler have a thicker TPS but reduced thermal mass of the substructure (dark gray areas in Fig. 12). CFD simulations without radomes indicate that peak heat load for these regions occur on the PCC's leeside near the top edge. This location is not a real physical location as it lies under the TLGA; however, heat load at this location bounds heat load in similar regions calculated from CFD solutions with radomes. Therefore, sizing performed with leeside edge environments will be conservative for the regions without doubler/PUHF.

Megacutter (BP27): the two cutter closeouts are located at 10 and 2 o'clock positions. The additional layer of Aluminum results in reduced TPS thickness. Sizing is done for the cutter at 2 o'clock position (Megacutter) because it experiences higher heating due to RCS thruster plume interference. CFD environments at this location are augmented as described earlier. Sizing is done for the structure stack at the center of Megacutter where it overlays a cutout in PCC cone (lower thermal mass).

RCS 2 o'clock (BP15): MSL RCS-on simulations indicated that a location near the top of the cone at the 2 o'clock position experiences heating augmentation from RCS plume. Given the proximity of this location to the leeside edge sizing location, analysis was performed at this location with RCS-augmented environments to ensure that the addition of RCS heat load does not drive TPS sizing for this region.

As shown earlier in Fig. 11, most of the aerothermal analysis for Mars 2020 was done on smooth-OML CFD grid that did not include protrusions like TLGA and PLGA. A few simulations (a subset of trajectory points) were performed using a grid that included the radomes. The heating environment used in Acusil-II sizing for TLGA and PLGA were derived from these simulations, extracted at the peak heating location on each radome. These sizing locations are labeled as BP22 and BP25 in the results table.

Since the radome CFD simulations showed areas of localized heating downstream of the TLGA, two additional sizing cases were considered at the base of TLGA radome. TLGA astroquartz structure is attached as a separate hardware on PCC cone resulting in two distinct regions at the base of the radome, one region without aluminum backing but with higher bondline temperature limit and another for the region that overlaps the PCC cone but with lower bondline temperature limit driven by aluminum allowable. These two sizing locations were named "TLGA Base Lee" and "TLGA Base PCC" and are labeled as BP23 and BP24.

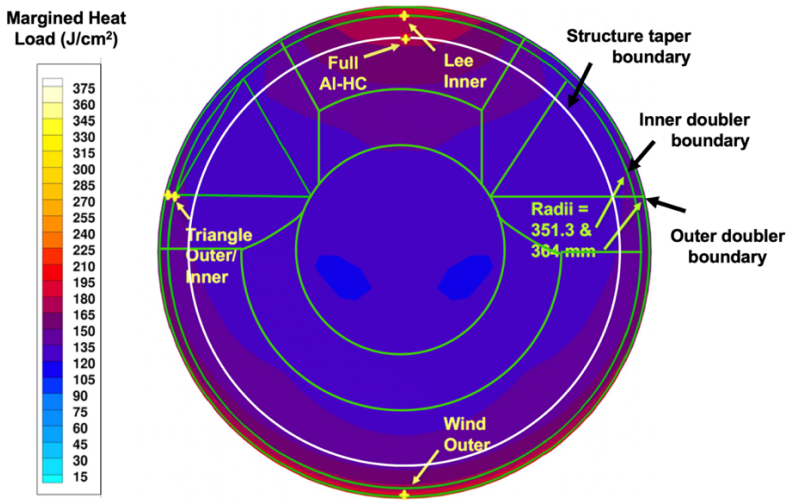


**Fig. 13 Lid heat load contours overlaid on structure/TPS thickness boundaries showing sizing locations**

In an attempt to identify the sizing locations that had to be considered for the lid TPS, boundaries showing variations in Acusil-II thickness and structure stack (shown earlier in Fig. 6) were overlaid on the lid's heat load contour map. This is shown in Fig. 13. The white circle displays the radial location where the aluminum honeycomb

structure starts tapering to only facesheets. As mentioned earlier, doublers with varying thicknesses are installed in the facesheet region for structural reasons. Two green circles are also shown in this figure labeled as "inner" and "outer". The area between the white circle and this inner boundary has the minimum doubler thickness while the area between inner and outer boundaries has the maximum doubler thickness. Additionally, variations in Acusil-II thickness are shown with green boundary lines. The two arc-shaped regions on the windside and leeside have the maximum Acusil-II thickness while the central circle and the two triangular regions on either side have the minimum Acusil-II thickness. These regions are connected to each other using linear and cylindrical ramps. Given the variations in surface heating, structure stack and Acusil-II thickness, a total of five sizing cases were considered.

Full Al-HC (BP21): This sizing case corresponds to the region where the lid has the full thickness of the aluminum honeycomb before it tapers. Acusil-II thickness varies from 0.74 cm to 0.96 cm. Max heating within this region occurs on the leeside as identified by the heat load map in Fig. 13. If one can show that the sized thickness with maximum heating environments is less than the minimum design thickness of 0.74 cm, it is guaranteed that Acusil-II thickness is sufficient for the entire area where the full thickness of aluminum honeycomb is present (majority of the lid).

Windside Outer (BP16): This sizing case corresponds to the maximum heating location within the facesheet-only areas in the lid where both the doubler and Acusil-II have their maximum thickness. The peak heating in this region occurs on the windside and is used in sizing.

Leeside Inner (BP19): This sizing case corresponds to the maximum heating location within the facesheet-only areas in the lid where Acusil-II has its maximum thickness, but the doubler can have its minimum thickness. The peak heating in this region occurs on the leeside and is used in sizing.

Triangle Outer (BP17): This sizing case corresponds to the maximum heating location within the facesheet-only areas in the lid where the doubler has its full thickness, but Acusil-II can have less-than-maximum thickness. The peak heating in this region occurs in the triangular area. Sizing results are assessed against the minimum Acusil-II thickness of 0.74 cm (conservative choice to minimize number of sizing cases).

Triangle Inner (BP18): This sizing case corresponds to the maximum heating location within the facesheet-only areas in the lid where the doubler can have its minimum thickness and Acusil-II can have less-than maximum thickness. The peak heating in this region occurs in the triangular area. Sizing results are assessed against the minimum Acusil-II thickness of 0.74 cm (conservative choice to minimize number of sizing cases).

It was mentioned earlier that absorptivity was set to the maximum possible value of 1.0 for PICA and SLA sizing due to lack of reliable data. This conservative approach was not pursued for Acusil-II given that radiative heating is a larger contributor of total heating on PCC/BIP and the fact that the design thickness was not expected to have large margins. Limited reflectance measurements of Acusil-II were made at varying wavelengths in the early 1990's by Aerotherm Corporation [18]. This data was used to derive an absorptivity estimate, which was margined by 10% to account for uncertainties in the data and limitations in the analysis approach. A final absorptivity value of 0.832 was used in this analysis.

*4. Sizing Results*

Fig. 14 shows a pictorial representation of the Mars 2020 TPS sizing locations discussed earlier in this paper. The numbers in this figure denote the body point number for each sizing location. This includes one location on the heatshield, two locations on the backshell and 17 locations on the PCC/BIP.

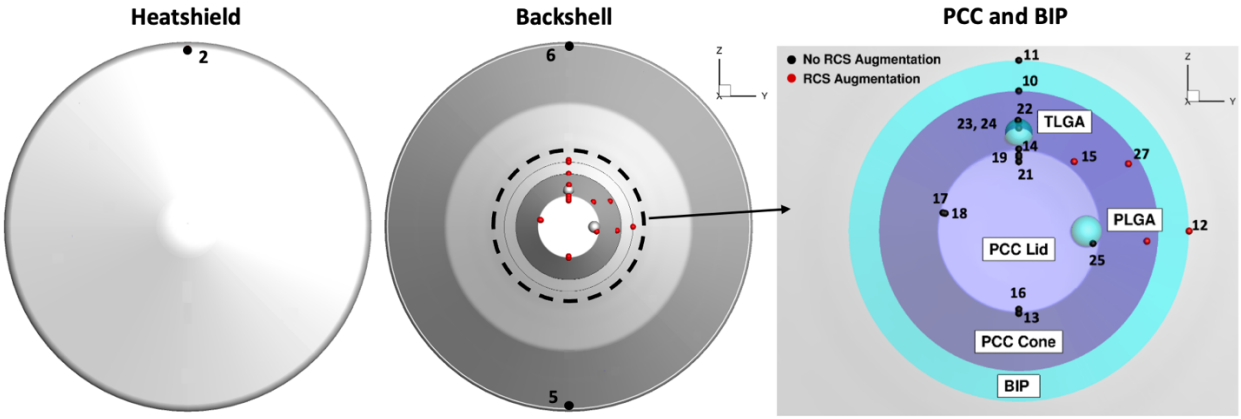


**Fig. 14 Summary of Mars 2020 TPS sizing locations**

Table 3 reviews certain key assumptions employed in TPS sizing and margining process. Bondline temperature limits, bondline temperature margins (derived from Monte Carlo analysis done for each sizing location), initial temperatures at entry interface and manufacturing tolerances are listed for each sizing location. Table 4 shows a summary of sized thicknesses and how they compare with the design thicknesses at each sizing location.

**Table 3 Assumption employed in Mars 2020 TPS sizing**

| Sizing Case | Body Point | Bond. Temp. Limit (°C) | Initial Temp. (°C) | Bond. Temp. Margin (°C) | Manufacturing Tolerance (cm) |
|---|---|---|---|---|---|
| Heatshield Max Q | 2 | 177 | -48 | 57.7 | 0.051 |
| Backshell Wind Seal | 5 | 150 | -31 | 27.4 | 0.076 |
| Backshell Lee Seal | 6 | 150 | 4 | 23.6 | 0.076 |
| BIP Lee PCC | 10 | 55 | 35 | 5.4 | 0.025 |
| BIP Lee BS | 11 | 55 | 35 | 5.8 | 0.025 |
| BIP Side RCS | 12 | 55 | 35 | 5.8 | 0.025 |
| PCC Windside Edge | 13 | 150 | 35 | 15.7 | 0.025 |
| PCC Leeside Edge | 14 | 150 | 35 | 16.9 | 0.025 |
| PCC RCS 2 o'clock | 15 | 150 | 35 | 16.9 | 0.025 |
| PUHF Antenna | 13 | 180 | 35 | 24.8 | 0.025 |
| Megacutter | 27 | 150 | 35 | 16.0 | 0.025 |
| TLGA | 22 | 230 | 35 | 35.1 | 0.025 |
| TLGA Base Lee | 23 | 230 | 35 | 31.3 | 0.025 |
| TLGA Base PCC | 24 | 150 | 35 | 15.6 | 0.025 |
| PLGA | 25 | 230 | 35 | 43.8 | 0.025 |
| PCC Lid Full Al-HC | 21 | 230 | 25 | 23.7 | 0.025 |
| PCC Lid Wind Outer | 16 | 230 | 25 | 29.5 | 0.025 |
| PCC Lid Lee Inner | 19 | 230 | 25 | 28.9 | 0.025 |
| PCC Lid Trian. Outer | 17 | 230 | 25 | 30.5 | 0.025 |
| PCC Lid Trian. Inner | 18 | 230 | 25 | 27.2 | 0.025 |

**Table 4 Mars 2020 TPS sizing results**

| Sizing Case | Body Point | Nominal Thick. (cm) | Aerothermal Thick. (cm) | Thermal Thick. (cm) | Sized Thick. (cm) | Design Thick. (cm) | Design FOS |
|---|---|---|---|---|---|---|---|
| Heatshield Max Q | 2 | 1.44 | 1.54 | 1.81 | 2.02 | 3.05 | 1.52 |
| Backshell Wind Seal | 5 | 0.48 | 0.67 | 0.57 | 0.84 | 1.27 | 1.72 |
| Backshell Lee Seal | 6 | 0.50 | 0.62 | 0.60 | 0.80 | 1.27 | 1.83 |
| BIP Lee PCC | 10 | 1.57 | 1.94 | 1.84 | 2.25 | 2.45 | 1.20 |
| BIP Lee BS | 11 | 1.60 | 2.00 | 1.87 | 2.31 | 3.97 | 1.90 |
| BIP Side RCS | 12 | 1.49 | 1.91 | 1.78 | 2.22 | 3.97 | 1.98 |
| PCC Windside Edge | 13 | 0.26 | 0.80 | 0.37 | 0.92 | 1.50 | 1.82 |
| PCC Leeside Edge | 14 | 0.84 | 1.43 | 1.03 | 1.63 | 1.74 | 1.18 |
| PCC RCS 2 o'clock | 15 | 0.72 | 1.17 | 0.88 | 1.34 | 1.74 | 1.43 |
| PUHF Antenna | 13 | 0.28 | 0.64 | 0.38 | 0.75 | 1.29 | 1.93 |
| Megacutter | 27 | 0.61 | 1.07 | 0.76 | 1.23 | 1.64 | 1.48 |
| TLGA | 22 | 1.13 | 1.79 | 1.44 | 2.06 | 2.50 | 1.34 |
| TLGA Base Lee | 23 | 0.17 | 0.51 | 0.30 | 0.61 | 1.59 | 2.96 |
| TLGA Base PCC | 24 | 0.33 | 0.71 | 0.45 | 0.83 | 1.59 | 2.14 |
| PLGA | 25 | 1.23 | 1.78 | 1.44 | 2.03 | 2.50 | 1.36 |
| PCC Lid Full Al-HC | 21 | 0.24 | 0.56 | 0.31 | 0.65 | 0.74 | 1.26 |
| PCC Lid Wind Outer | 16 | 0.13 | 0.51 | 0.25 | 0.61 | 0.96 | 1.76 |
| PCC Lid Lee Inner | 19 | 0.36 | 0.78 | 0.48 | 0.90 | 0.96 | 1.17 |
| PCC Lid Trian. Outer | 17 | 0.06 | 0.42 | 0.18 | 0.51 | 0.74 | 1.64 |
| PCC Lid Trian. Inner | 18 | 0.28 | 0.65 | 0.39 | 0.76 | 0.74 | 1.07 |

Table 4 provides the sized thicknesses from each sizing branch in the margin flow chart shown earlier. "Nominal Thickness" represents the required thickness without applying aerothermal and thermal margins, while "Aerothermal Thickness" and "Thermal Thickness" represent the required thicknesses after applying the aerothermal and bondline temperature margins respectively. These thicknesses are combined according to Equation 1, shown earlier, followed by the addition of recession margin (applicable only for the heatshield), 10% factor of safety, and manufacturing tolerance to arrive at the "Sized Thickness" shown in the sixth column. The design thickness at each sizing location is shown in the seventh column. The actual factor of safety for the design thickness is also calculated based on Equation 2 shown earlier. This represents the amount of extra TPS available in the design thickness beyond what is required by thermal sizing. The design thickness is sufficient at all sizing locations and the required minimum factor of safety of 1.1 is met. The only case with less than 1.1 factor of safety is the "Triangle Inner" sizing location on the PCC lid which represents the region where both Acusil-II and facesheet doubler simultaneously have their minimum thicknesses. Further evaluation of the design in this region confirmed that this small area is surrounded by regions with higher thermal mass including thicker doubler, thicker Acusil-II and tapered aluminum honeycomb. While the one-dimensional analysis presented here shows a factor of safety lower than 1.1, a multi-dimensional analysis would certainly show a substantially lower sized thickness due to the in-plane conduction and surrounding thermal mass. Additionally, the 1.1 factor of safety guideline is usually recommended for analysis in early design cycles to provide margin for potential changes in vehicle design and environments. Given the conservative nature of the sizing methodology used here and the fact this analysis is done based on final vehicle design parameters, a factor of safety greater than 1 is considered adequate.

## V. Arcjet Testing and Analysis

A total of six arcjet test series were performed by the Mars 2020 project in the Panel Test Facility (PTF) and Interaction Heating Facility (IHF) at NASA Ames Research Center. Below is a list of these arcjet tests.

1. IHF 348 – PICA wedge panels with and without discoloration in IHF 6-inch nozzle
2. PTF 158 – PICA panels in PTF with in-depth thermocouples within discolored and nominal regions
3. IHF 358 – PICA flight-lot wedge panels in IHF 6-inch nozzle
4. IHF 361 – PICA flight-lot stagnation coupons in IHF 13-inch nozzle
5. PTF 163 – SLA-561V flight-lot panels in PTF
6. PTF 163 – Acusil-II flight-lot panels in PTF

IHF 348 and PTF 158 were risk reduction tests, conducted earlier in the program, that were linked to surface and in-depth discolorations observed in flight-lot PICA material during manufacturing and tile machining. A detailed study was conducted to show that the discoloration in PICA did not negatively impact its properties and thermal response. This included microscopic imaging, thermal property testing, and arc jet testing in both wedge and panel configurations. The wedge testing was aimed at evaluating PICA recession performance under high heat flux and shear conditions by comparing recession of test coupons containing discolored material with coupons with nominal material and against historical test data. The panel testing focused on obtaining surface and in-depth temperature data at lower conditions to compare the in-depth response of discolored material with nominal material and verify its agreement with analytical model predictions. Details of the PICA discoloration study is outside the scope of this paper; nevertheless, this investigation concluded that there were no significant differences in the thermal response of discolored PICA compared to the regular PICA material. This conclusion allowed the use of tiles with discoloration on the flight vehicle. Tiles with discoloration can be seen near the heatshield shoulder in Fig. 1.

The remaining four tests were part of the flight-lot acceptance campaign which were conducted later in the program using test articles that were built with the same materials and at the same time as the installation of flight TPS on the aeroshell (made from witness panels). The main objective of flight-lot acceptance testing is to verify the workmanship of flight TPS installation and demonstrate that the flight-lot TPS materials perform as expected and their thermal response is predicted by the analytical models used in TPS sizing and design.

The flight-lot testing for the heatshield was done in two distinct formats: shear wedge articles (IHF 358) and stagnation articles (IHF 361). Within each test series both PICA-only ("Acreage") and gap-filled ("Gap") configuration models were tested. Similar to the discolored PICA tests, the wedge tests allowed assessment of the material performance (particularly its recession behavior) at peak heat flux and shear conditions, while stagnation testing allowed for assessment of the thermal response of the full TPS and structure stack-up thermal response at peak heat flux and pressure conditions. The models for both the wedge and stagnation articles were instrumented at bondline location to provide basic information about the thermal response during the exposure. High-definition video,

pyrometer, and infrared camera data was collected to observe thermal and material response at the surface. More details about these tests are provided in Sections V-A and V-B.

The flight-lot testing for the backshell TPS materials were conducted in the PTF facility. PTF allows testing of large panels at lower conditions that are representative of Mars 2020 backshell environments. Details of Acusil-II flight lot test are described in Section V-C.

SLA-561V flight lot testing was also conducted in the PTF as a part of the same test series. This test was planned and executed by Lockheed Martin engineers; therefore, this paper provides only a brief description of the test. Two conditions that were representative of the predicted backshell environments were targeted: 13.5 W/cm$^2$ (high) and 5.2 W/cm$^2$ (low). Five panels of SLA-561V were tested in three configurations that included features intended to evaluate repairs and non-conformances that were encountered during the manufacturing of the flight aeroshell. The acreage TPS on all panels was packed alongside the flight backshell with flight material. One configuration included plug and edge repairs while another configuration contained repairs employed on the backshell door frame seal. The third configuration attempted to test SLA samples from the flight backshell. These samples came from areas which were intended to be removed following TPS installation and were incorporated into the test article acreage TPS as plugs. The objective for this configuration was to demonstrate that processing non-conformances that occurred during the packing of SLA on the flight backshell do not affect TPS performance. All panels tested successfully, and no adverse behaviors were observed. The material's performance was in-family with testing of SLA-561V conducted for the MSL program. This test verified that the non-conformances and repairs encountered during the flight backshell build had no impact on the performance of the TPS.

### A. PICA Flight Lot Stagnation Testing – IHF 361

6-inch flat-face articles, depicted in Fig. 15**,** were constructed with a flight-like stack-up of PICA, RTV-560 gap filler, and an aluminum honeycomb and facesheet composite substructure. One of the test articles included a gap filler repair that was implemented on the flight heatshield. Inspection of gap fillers on the flight vehicle revealed voids that were larger than the maximum size allowed. These voids were present both in-depth and near the surface. Regions with large in-depth voids were fixed using a repair plug technique that was developed and qualified by the MSL program [22]. However, the voids that were closer to the surface were repaired by carving out the RTV region with voids and refilling the cavity with RTV. This surface fill technique sometimes resulted in regions that were locally wider than the design gap width. Another concern was the integrity of the bond between the freshly added RTV and the previously cured RTV. Two types of surface fill repairs were implemented in one of the models, as shown in Fig. 15a, to verify the performance of this new repair technique. The models were also instrumented with Type-K (K#) thermocouples placed at various TPS and structure interfaces, as shown in Fig. 15b.

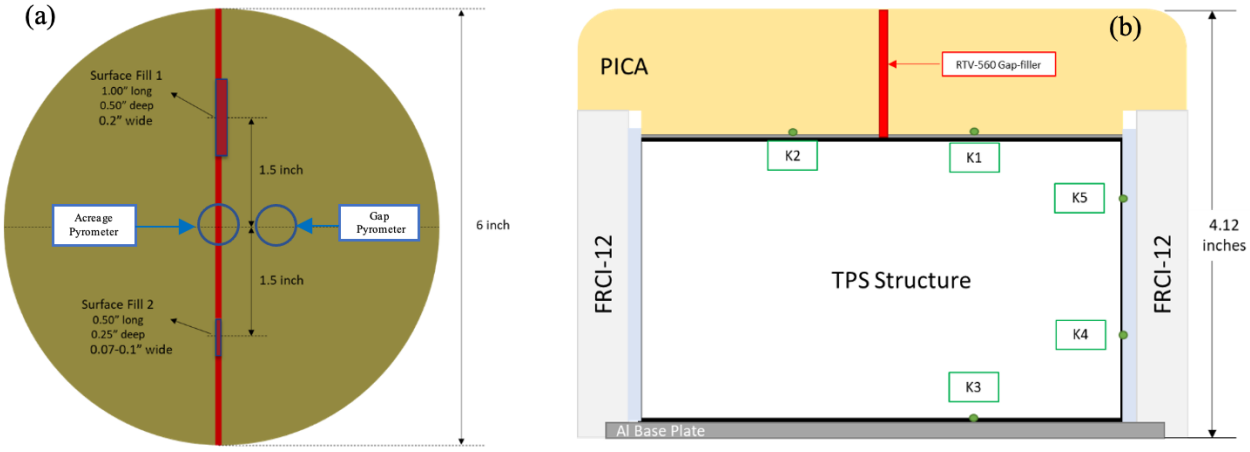


**Fig. 15 Model gap-filler layout, Gap Repair details, and PICA-TPS stack-up with general thermocouple placement**

The conditions listed in Table 5 target the peak forebody heat flux and the 40% peak heat flux condition. Both conditions were run with similar heat load by changing exposure length. In addition to the arc jet conditions, this test series also performed a cold soak operation on select models to simulate to temperatures that would be experienced during cruise, followed by the atmospheric entry pulse. The cold soak operation was performed by submerging the model, wrapped in Mylar film, in liquid nitrogen to cool the model to approximately -150 °C. After reaching the

desired temperature, the model would quickly be installed by facility technicians to the model sting arms, and the test box would be closed, allowing the chamber to pump down to vacuum levels and perform the arc jet test. For each model under the cold soak, the temperature before arc jet exposure was approximately -50 °C before arc jet exposure. Fig. 16 shows pre and post-test images of the gap model tested at the low condition. Recession is limited 3 mm for models exposed to the High condition and approximately 1.7 mm for models exposed to the Low condition, excepting the RTV-560 gap-filler which did not recede as much, shown in Fig. 16c. RTV is known to swell and recede at different rates than the surrounding PICA, specially at low conditions, creating a raised region at the gap (often referred to as "RTV Fencing").

**Table 5 IHF 361 Arc jet test model configuration and condition summary**

| Model Configuration | Model ID | Starting Condition | Cold Wall Heat Flux [W/cm$^2$] | Duration [s] | Pressure [kPa] |
|---|---|---|---|---|---|
| Acreage | 501-002 | Cold Soak | 210 (High) | 33 | 17 |
| | 501-003 | Ambient | | | |
| Gap | 502-002 | Cold Soak | | | |
| | 502-003 | Ambient | | | |
| Gap Repair | 505-001 | Cold Soak | | | |
| Acreage | 501-001 | Ambient | 84 (Low) | 65 | 20 |
| Gap | 502-001 | Ambient | | | |

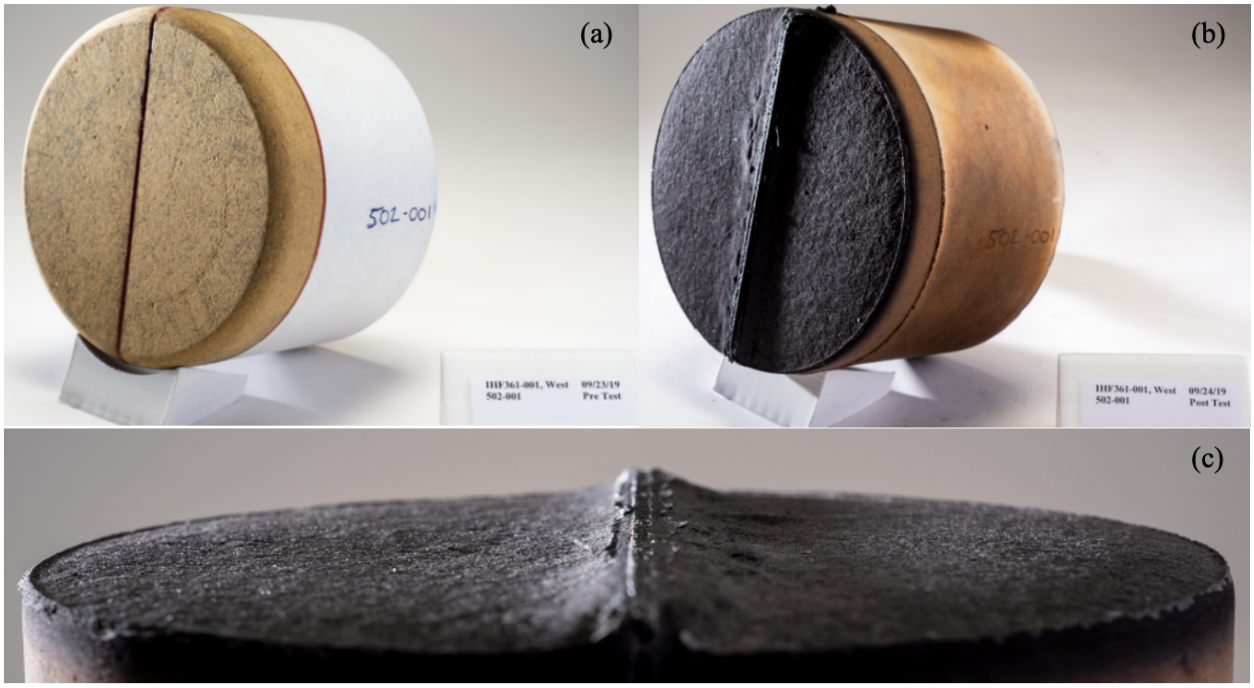


**Fig. 16 Gap Model (502-001) pre-test (a) and post-test (b) photographs with surface gap-filler detail (c)**

Fig. 17 shows the bondline thermocouple time history (TC1) for all models subjected to a cold soak and starting from ambient conditions. For each condition, the models experienced consistent surface temperatures at approximately 1600 °C and 2100 °C for the Low condition and High condition, respectively. It was observed during testing that the coating that was sprayed on the heatshield, NuSil, was melting and flaking off the surface of the PICA. This process had a small, but noticeable impact on the surface temperature in the first moments of exposure to the arc jet. The effect is seen in the small slope change of the temperature for the High condition just after insertion and at approximately 10 s into exposure for the Low condition. The model bondline thermocouples measured a consistent response, increasing by 100-120 °C during the test, depending on the model initial temperature. At the Low condition, the Gap and Acreage display similar bondline temperatures while at the High Condition the Gap model displays a lower bondline. Under Cold Soak conditioning, the RTV-560 Gap Repair model performed similarly to the Acreage model

and measured a lower temperature than the other Cold Soak Gap model tested at the High condition. For all runs, no model failures or flaws were uncovered.

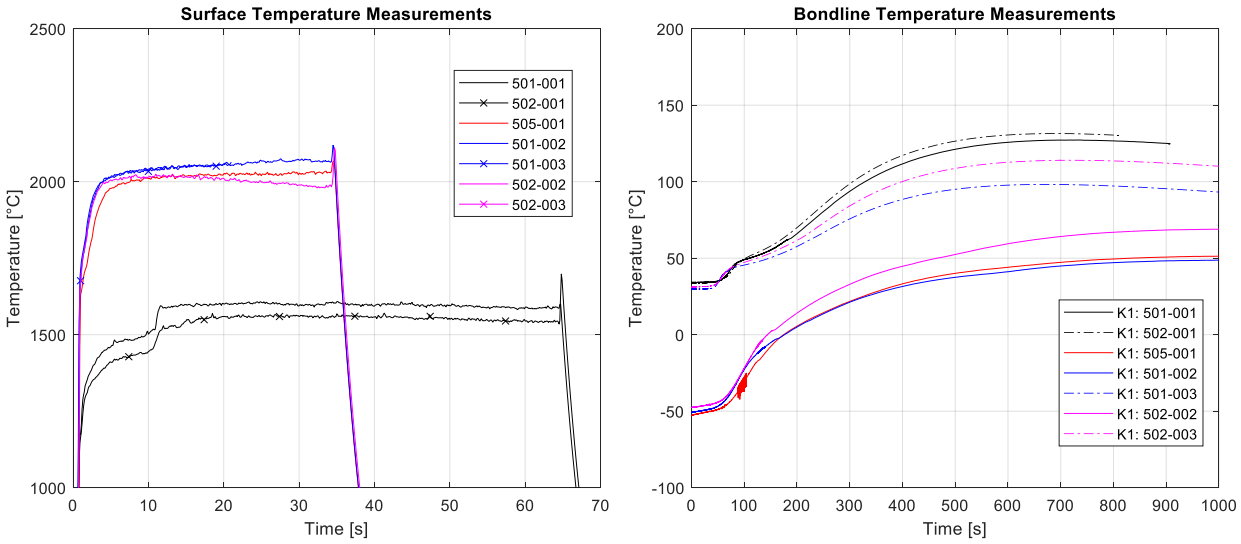


**Fig. 17 (Left) Two-color pyrometer surface temperature measurements for each model and (right) bondline thermocouple measurements from K1**

## B. PICA Flight Lot Acceptance Wedge Testing – IHF 358

Wedge models with TPS running length of approximately 4 inches and 20° inclination with respect to the oncoming arc jet flow were tested in the IHF using the 6-inch nozzle at facility maximum conditions. Both Acreage and Gap models were tested. The model and condition summary are listed below in Table 6. The conditions were chosen to get close to the predicted design heat flux, pressure, and shear values. Since shear cannot currently be measured directly in the facility, CFD calculations were performed post-test to demonstrate that flight-like environments were achieved. Fig. 18 shows a diagram of the stack-up and construction of the wedge models. The location of bondline thermocouples (K1 and K2) and the region where pyrometers were targeted at are also shown in this figure.

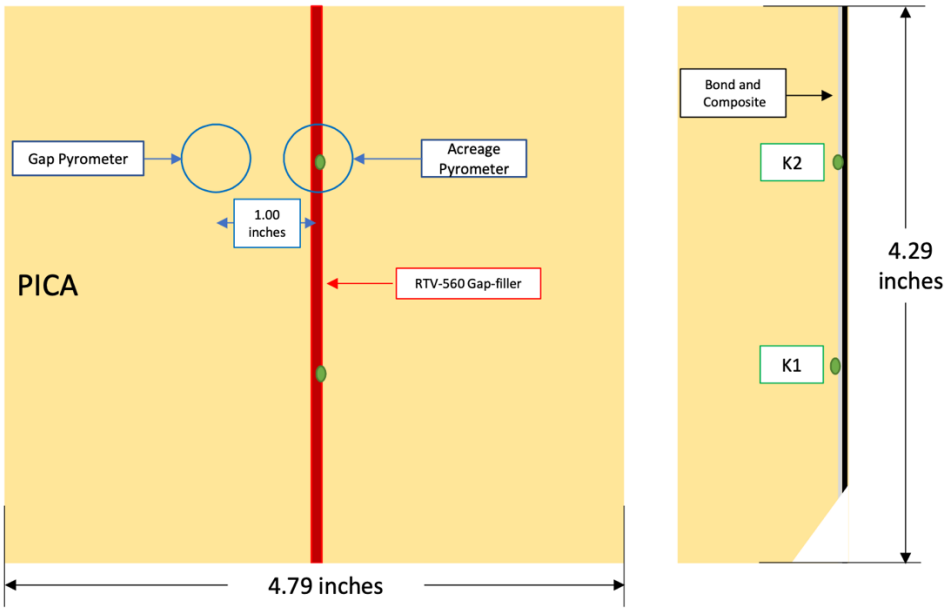


**Fig. 18 Model layout, and PICA-TPS stack-up with general thermocouple and pyrometer placement**

Fig. 19 shows pre-test pictures of the assembled models and their corresponding post-test state. Both the acreage and gap filler models performed as expected and consistent with past PICA testing at this condition. The streak lines observed in the post-test pictures are a product of the non-uniform flow patterns over the wedge model and is not indicative of non-uniformity in PICA material response.

**Table 6 IHF 358 model configuration and arc jet condition summary**

| Model Configuration | Model ID | Cold Wall Heat Flux [W/cm$^2$] | Duration [s] | Shear Stress [Pa] | Pressure [kPa] |
|---|---|---|---|---|---|
| Acreage | 503-004<br>503-007 | 175-300 | 21 | 300 - 400 | 14 - 26 |
| Gap | 504-002<br>504-003 | | | | |

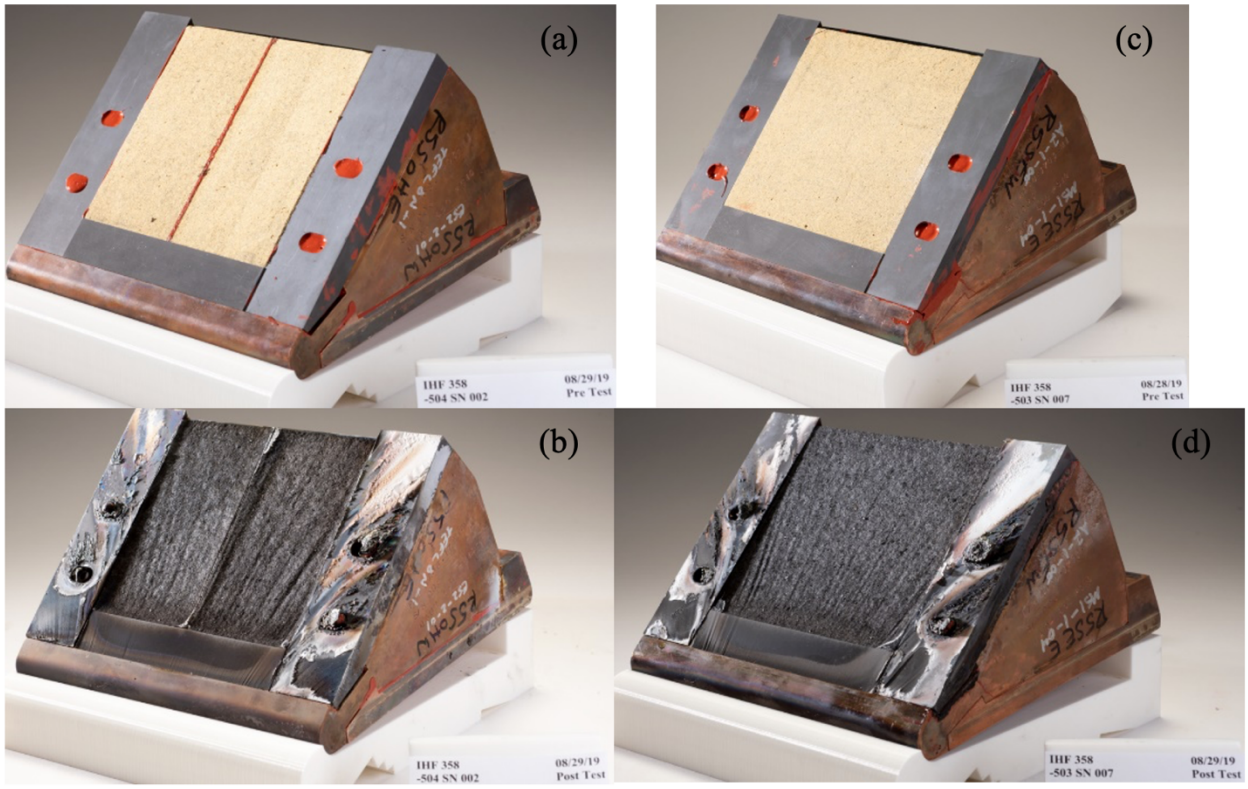


**Fig. 19 (a) Pre-test Gap model S/N: 002 assembled into 20° water-cooled wedge. (b) Post-test Gap model S/N: 002. (c) Pre-test Acreage model S/N: 007 and (d) post-test Acreage model S/N: 007**

Locations shown in Fig. 18 were targeted for pyrometry and bondline thermocouple temperatures were recorded. Displayed in Fig. 20, the thermocouple traces for each model show that the in-depth temperature rose faster for the Acreage models than for the Gap models. This is expected since the RTV-560 is denser and acts as a heat sink. Long-term temperature trends and final values, however, cannot be assessed since the model is not insulated against the water-cooled copper which creates and indeterminate boundary condition beneath the model. Unlike the stagnation test series where NuSil coating slowly flaked and melted away accompanied with a distinct change in measured surface temperature, the coating ablates away quickly in the wedge testing and a step increase in surface temperature was not observed.

As part of the post-test characterization, laser scan measurements were taken to quantify the recession of the PICA and RTV-560 gap-filler. The entire models were scanned, and cross-section measurements were extracted for a spanwise measurement, 1 inch from the model downstream edge, seen in Fig. 21. Since both IHF 348 and IHF 358 were run at the same facility settings and experienced similar conditions, a comparison was performed between the recession measurements from the discolored PICA test (called “Dark PICA” in this figure) and the flight-lot test. The

recession data shows that discolored PICA and flight lot PICA respond in a similar manner, with the recession measurements in very good agreement. Recession elsewhere on the models was limited to 3 mm. Similar to the stagnation test, RTV fencing can be observed along the wedge centerline. Furthermore, no flaws or failure in either the PICA or RTV-560 gap-filler were observed during the testing.

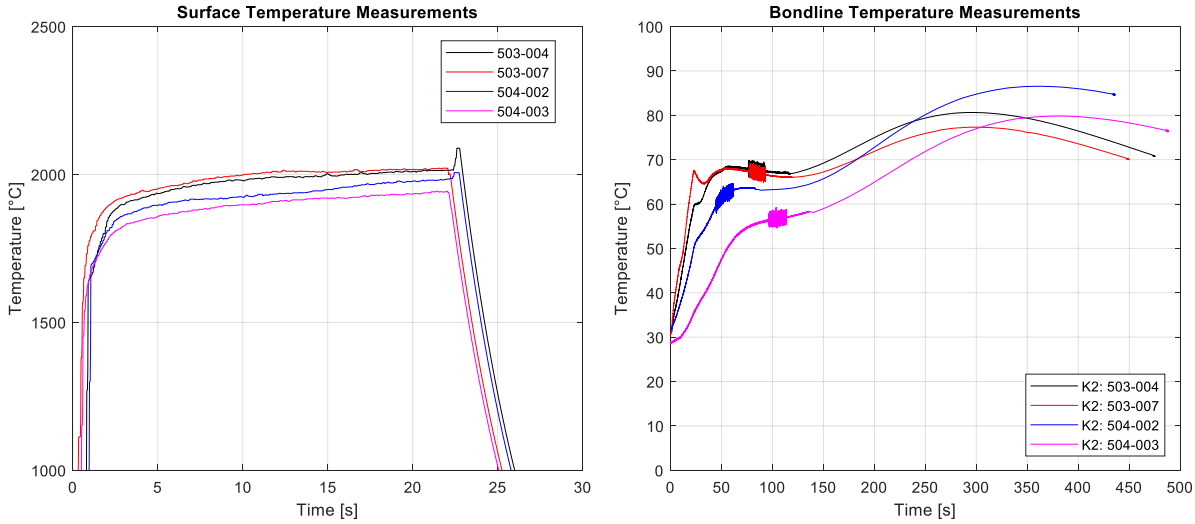


**Fig. 20 (Left) two-color surface pyrometer measurements and (right) downstream bondline thermocouple TC2 measurements**

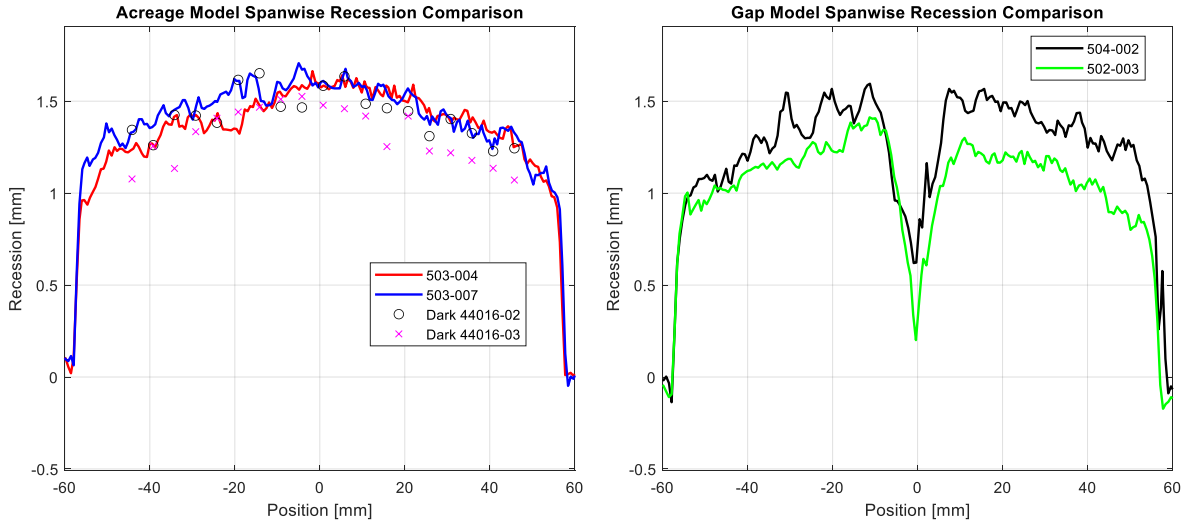


**Fig. 21 (Left) IHF 358 Acreage Flight Lot PICA and IHF348 Dark PICA recession comparison and (right) Gap model recession comparison. Dark PICA measurements were made manually while IHF358 measurements were made using a laser scanner**

### C. Acusil-II Flight Lot Acceptance Test – PTF 163

Two panel configurations were tested in the Acusil-II flight lot test series. One configuration, named "PCC Panel", used an aluminum substrate which was representative of PCC's structure, while the other configuration, named "PLGA Panel", used an astroquartz substrate which was representative of the antenna radomes. In the PTF, the primary value of interest is the heat flux, tested for a duration to match the heat load. A water-cooled Gardon Gage calorimeter plate is used to set the necessary facility parameters, and experiences cold wall heat flux that is estimated to be approximately 5 - 10% higher than the predicted hot wall heat flux. In the PTF, the table angle is set to a minimum angle of -6° from parallel to the nozzle centerline. As such, when the arc jet is turned on, the model is exposed to

lower level of heating from the plasma. The table angle is set to the desired setting at time, t= 0 s. After the model has been exposed for the desired duration, the table angle is set back to the minimum setting while the arc jet begins its shutdown, continuing to expose the model to heated gas. The test for the panels is therefore an over-test on heat load.

Two conditions were set for this test: a high condition that simulates the heating experienced at the PLGA region and RCS thruster-augmented heating regions on the PCC/BIP, and a low condition that targets the peak heating estimated on the PCC. The estimated cold wall heat flux, duration, and pressure values are shown with the test configuration in Table 7.

**Table 7 PTF163 Acusil-II model configuration and arc jet condition summary**

| Model Configuration | Model ID | Cold Wall Heat Flux [W/cm$^2$] | Duration [s] | Pressure [kPa] |
|---|---|---|---|---|
| PCC Panel | M2020-001<br>M2020-002 | 8.8 | 41 | 1.27 |
| PLGA Panel | M2020-003<br>M2020-004 | 14.0 | 41 | 1.22 |

As shown in Fig. 22, both panels are composed of a 12-inch square piece of Acusil-II bonded to the substrate. The Acusil-II thickness is 1.00 and 0.725 inches on the PLGA and PCC panels, respectively. The location of bondline thermocouples and the region where pyrometers were targeted at are also shown in this figure. Due to manufacturing issues, the Acusil-II thickness on the PLGA panel was as low as 0.92 inches in certain regions.

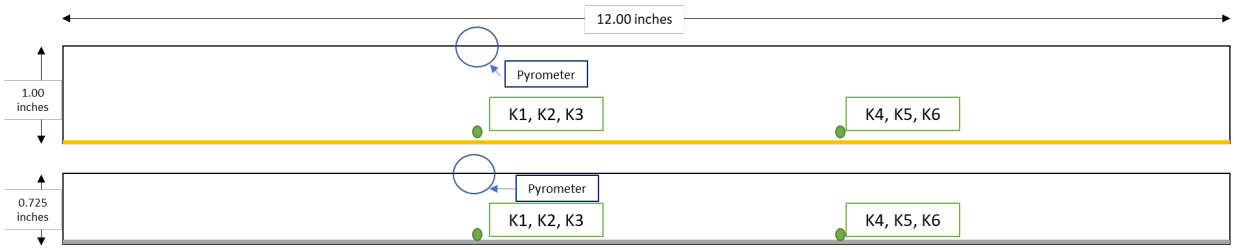


**Fig. 22 (top) PLGA Acusil-II panel. (bottom) PCC Acusil-II. Co-located thermocouples are at the same dimension from leading edge, spaced 3 inches apart with TC2 and TC5 on model centerline**

Fig. 23 shows pre-test and post-test images of both panels. The TPS performed successfully without showing any flaws or failures. Surface temperature and thermocouple response for each of the tested articles is shown in Fig. 24. For each model, the bondline temperature shows that the maximum allowable of 150°C for the PCC and 230°C for the PLGA was not exceeded. For model M2020-001, the low-temperature pyrometer experienced an error and did not return useable data. Model M2020-004 experienced a pop-out event where the model was blown partially down the test chamber, but the model was recovered and successfully retested. Notably, the surface temperature is seen to cool in each run during the arc jet exposure. This behavior may be explained by changes to the surface emissivity of the Acusil-II during test. As it chars and the surface blackens, the emissivity would increase and improve the heat rejection for the material. No significant recession was measured, as the Acusil-II material does not ablate at low heat fluxes, instead exhibiting small surface cracks.


**Fig. 23 (a) Pre-test PCC Acusil-II photograph and (c) post-test surface after exposure to Low condition (b) Pre-test PLGA Acusil-II photograph and (d) post-test surface after exposure to the High condition**

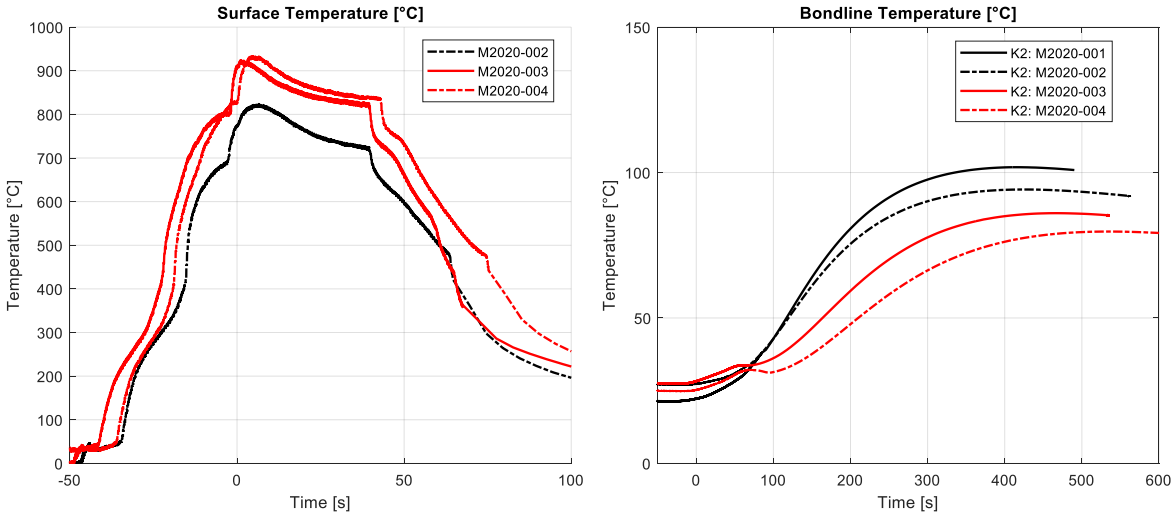


**Fig. 24 (Left) single-wavelength pyrometer (ϵ = 1.0) surface temperatures. (Right) bondline thermocouple temperatures for each model**

## D. Thermal Response Analysis

This paper includes thermal response analysis results for only IHF 361 (PICA stagnation flight lot) and PTF 163 (Acusil-II flight lot test). Although details are not discussed in this paper, FIAT analysis was performed for the discolored PICA test in PTF (PTF 158) and showed that the thermal response of the discolored PICA was well predicted by the PICA thermal response model. Thermal response analysis for the SLA-561V flight-lot test was performed by the aeroshell contractor, Lockheed Martin; however, it is not discussed in this paper.

FIAT analysis was not performed for the wedge tests (IHF 348 and 358). Data obtained from these tests are usually not suitable for verifying thermal response model predictions because IHF wedge panels typically have a leading edge

made of copper which results in excess oxygen in the boundary layer on PICA leading to different mass and heat transfer coefficients. Standard thermal response codes, including FIAT, assume equal transfer coefficients; therefore, they cannot match recession measurements from wedge testing accurately. Furthermore, since the wedge copper body is water-cooled, the thermocouples installed at PICA-wedge bondline are only suitable for detecting material failures (such as flow-through) or in-depth response that is significantly different from expectations. Their sensitivity/response is not sufficient for model verification unless the cooling mechanisms are accurately modeled. In these tests, the material response is usually evaluated by comparing to data from historical PICA testing and looking for any signs of failures and flaws.

*1. Thermal Analysis for PICA Flight Lot Stagnation Testing - IHF 361*

FIAT analysis was performed for the PICA stagnation test series using surface environments derived from CFD simulations that were verified against calorimeter data. Fig. 25 shows a comparison of FIAT recession predictions with measured recession at the test article centerline. We can see that the thermal response model accurately predicts recession for the flight-lot material at the high condition. However, at the low condition, we can see that FIAT overpredicts the measured recession significantly. The PICA thermal response model is known to overpredict surface recession at this range of conditions. The response model assumes thermal equilibrium for gas-surface interactions, but at low heat fluxes, surface conditions are not high enough to reach equilibrium and recession is limited by finite-rate reactions. This is exacerbated by the silicone surface coating applied to PICA coupons which inhibits recession in the beginning of the test before it vaporizes. The surface coating is also present on the coupons tested at the high condition; however, it vaporizes more quickly at high heat fluxes and therefore has a much smaller impact on the total recession values.

The overprediction of recession at the low condition may result in an inaccurate estimation of bondline temperature. Therefore, to allow for proper assessment of the in-depth response model independent of these surface modeling deficiencies, a second analysis approach is also considered here. In this approach, denoted as "FIAT option 2", FIAT surface boundary conditions are prescribed using surface temperature and recession rate. Surface temperature is derived by averaging pyrometer measurements. Recession rate is derived by dividing the total measured recession by the test duration. However, the first 12 seconds of the test are not included in the recession rate calculation because PICA does not recede until the NuSil coating is removed from the surface. This time is estimated using the sudden jump observed in pyrometer measurements when the coating has completely vaporized from the surface. The dotted blue line in Fig. 25 shows how the surface recession rate is prescribed in this analysis approach. Bondline temperature results will also be shown for the baseline approach used for the high condition, where surface boundary conditions are applied based on heating environments derived from CFD simulations that are tuned to match calorimeter measurements (denoted as "FIAT" in the following figures).

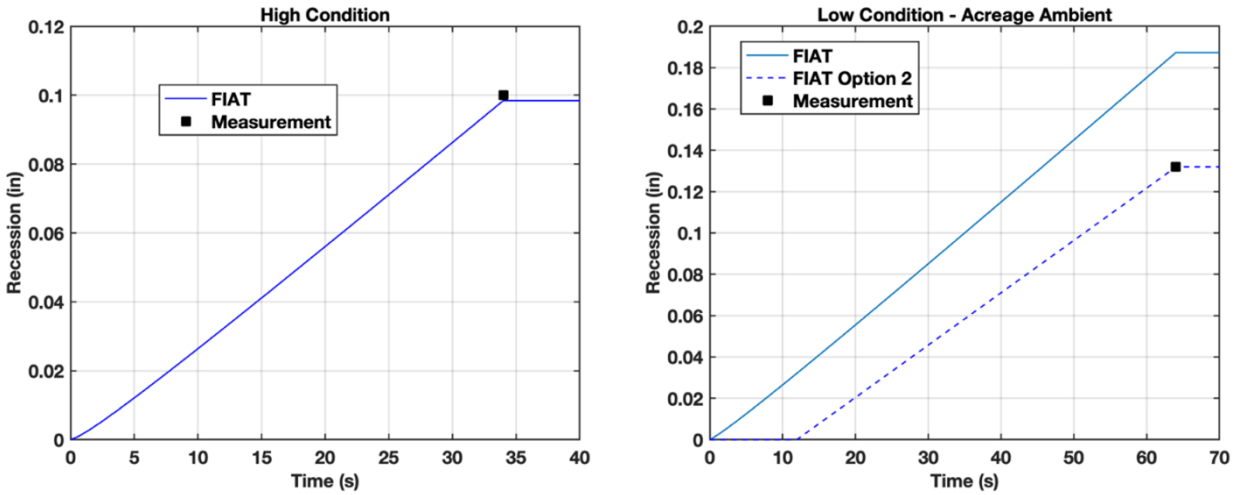


**Fig. 25 Comparison of PICA recession measurements and predictions for the high and low conditions**

Fig. 26 shows a comparison of the predicted bondline temperature with the thermocouple measurements for both conditions. For the high condition, we can see that the difference between peak bondline temperature measurement and FIAT prediction is less than 5 °C, which shows that the thermal response model accurately predicts the response

of the flight-lot material at this condition. For the low condition, the first thing to note is that the bondline temperature doesn't seems to be impacted significantly by the differences in the two analysis approaches. While the second analysis approach is marginally more accurate in resolving in-depth temperatures, it is obviously not critical for assessing the response model accuracy deep below the surface. It can be observed that the model underpredicts peak bondline temperature measurement regardless of which analysis approach is used. However, it should be noted that this underprediction is ~15 °C, which is far less than the 57 °C thermal margin used in heatshield TPS sizing which was applied to account for material property variants from one PICA billet to another. FIAT underpredicts the thermocouple measurements most likely due to the multi-dimensional effects that are not accounted for in FIAT's 1D analysis. These effects are expected to be more significant for the low condition where material's exposure to a relatively low heat flux for a long duration will allow more energy from the coupon's sidewalls and off-center regions to soak into the coupon and reach the thermocouples near the central region. A multi-dimensional analysis, not pursued in this work, can accurately capture these effects and show better agreement between predictions and data.

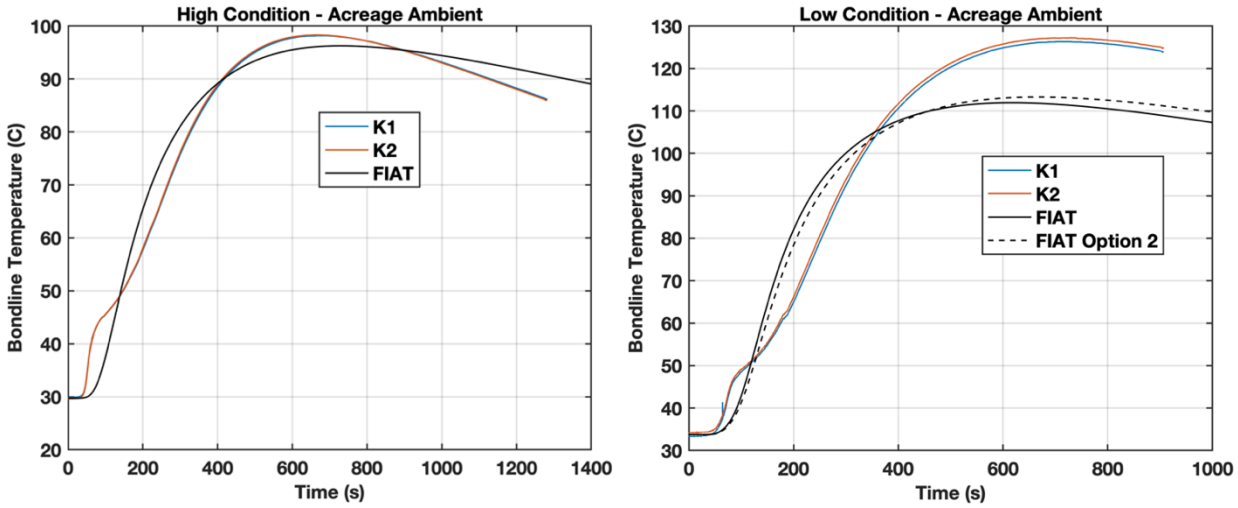


**Fig. 26 Comparison of predicted and measured PICA bondline temperature at high and low conditions**

*2. Thermal Analysis for Acusil-II Flight Lot Acceptance Test – PTF 163*

As mentioned before, during a test in PTF, a table holding the test panel is tilted up into the arcjet flow to attain the desired test conditions. However, the panel is continuously heated while in the lowered position from the time the arc is turned on and ramped up to condition until the table is tilted up. Once the desired exposure duration is reached, the table is lowered, but the panel continues to be heated until the arc is ramped down and turned off. Heating and pressure calibration measurements are usually done in a separate dedicated run using a panel equipped with heat flux and pressure gauges. The ramp up/down durations and steps during the calibration runs are often not the same as the runs including TPS panels, making it difficult to accurately estimate surface heating conditions before and after the main exposure period. This issue can be circumvented in thermal response modeling by using the measured surface temperatures from pyrometers as the surface boundary condition. Predicted bondline temperatures (using FIAT thermal response code) can be compared with the test measurements from bondline thermocouples to assess the accuracy of Acusil-II model in predicting the flight-lot material's response. This approach is identical to the analysis approach used for MSL Acusil-II flight-lot testing [23].

Fig. 27 compares the FIAT-predicted bondline temperature with measurements from multiple bondline thermocouples installed on the panel. The thermocouple measurements do not show much variation in peak bondline temperature across the panel. It can be seen that the Acusil-II thermal response model overpredicts the bondline temperature for both panels, confirming that the Acusil-II model is conservative for TPS sizing. This is consistent with observations from MSL flight-lot test. The shape of temperature profile for the PLGA panel is not as well-predicted as the PCC panel. This may be attributed to the lower thickness of Acusil-II for this panel, something that was noticed during its processing. Predictions with 0.92 inches of Acusil-II (minimum measured thickness across the panel) match the initial temperature rise better. The remaining differences may be attributed to the as-built thickness of astroquartz or the accuracy of astroquartz response model compared to that of aluminum (and consistency of astroquartz properties from one sample to another)

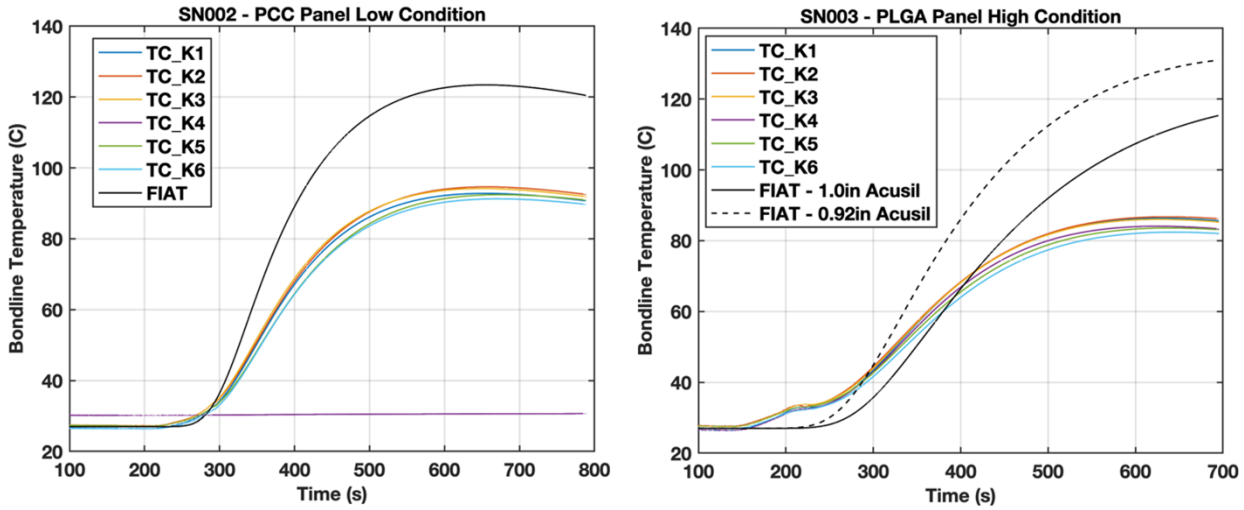


**Fig. 27 Comparison of Acusil-II bondline thermocouple measurements with FIAT predictions**

## VI. Comparison with Flight Temperature Data

Mars 2020 TPS materials were instrumented with a set of pressure, temperature and heat flux sensors called Mars Entry, Descent, and Landing Instrumentation (MEDLI2) [24]. This sensor suite included eleven MEDLI2 Instrumented Sensor Plugs (MISP) on the PICA heatshield and six MISP within the SLA-561V backshell, as shown in Fig. 28.

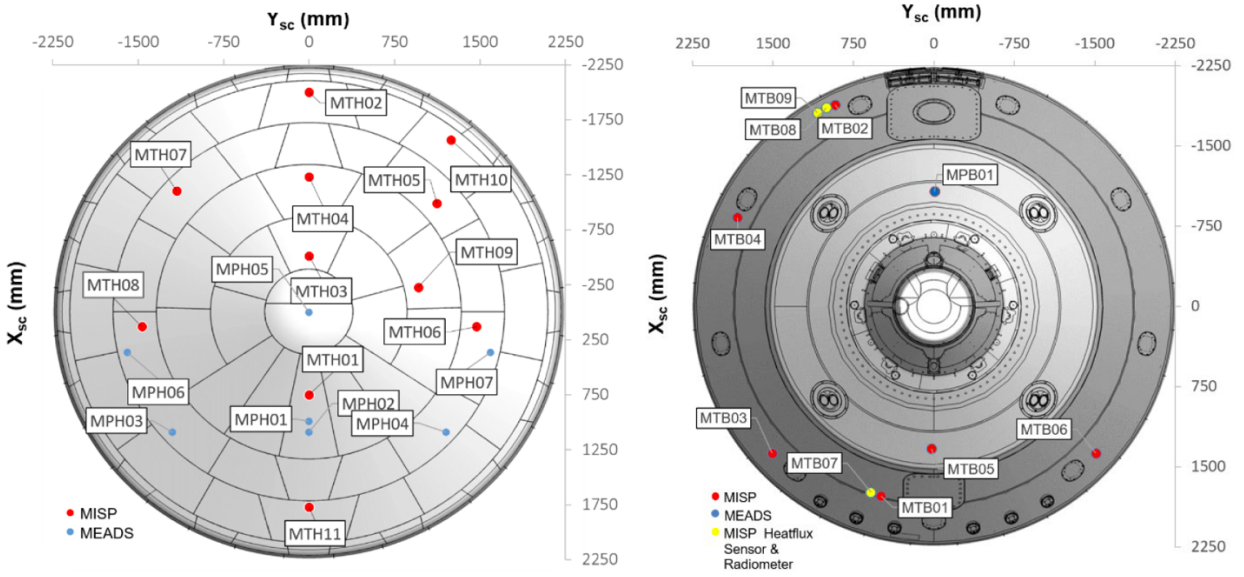


**Fig. 28 MEDLI2 sensor locations on the Mars 2020 heatshield (left) and backshell (right) [24]**

Post-flight analysis of the measured MISP data was compared to FIAT material response analysis to understand how well the Mars 2020 TPS sizing material models (PICA v3.3 and SLA-561V v1.0) predicted in-depth heating during entry. The substructure dimensions used in the FIAT analysis represent the as-flown dimensions at each MISP location. The TC depths were updated with X-ray analysis and the FIAT simulations updated the initial temperatures using the measured flight data to account for the measured thermal gradients through the TPS. In order to remove uncertainties in aerothermal boundary predictions and remove influence of coatings applied to the TPS, a "TC driver" modeling approach was chosen. The TC driver option does not use a surface energy balance equation since the wall

temperature and recession rate are input as a function of time in the FIAT environment file. The TC1 driver approach imposes the temperature of the TC nearest to the outer mold line of the vehicle as the surface boundary condition. FIAT in-depth temperature results are compared with the recorded MEDLI2 flight data in Fig. 29a (heatshield) and Fig. 29b (backshell). The first MISP data shown in Fig. 29a was placed on the leeside of the heatshield where elevated heating was expected. The MISP (MTH-02) was instrumented with three TCs at measured depths of 0.1953 cm, 0.5095 cm, and 1.1514 cm with ±0.0076 cm accuracy. The MISP data shown in Fig. 29b (MTB-01) was located on the windside backshell and included two TCs at 0.2563 cm and 0.6365 cm with ±0.0076 cm accuracy. Both the PICA and SLA-561V comparisons show that the material response modeling predicts higher in-depth temperatures than the MEDLI2 measured data. This suggests FIAT TPS sizing analysis provided conservative thicknesses which ensured the bondline temperatures remained below the temperature constraints defined during the Mars 2020 TPS sizing effort. A more complete comparison between measured flight data and pre-flight predictions is available in other published work [24], [25], [26].

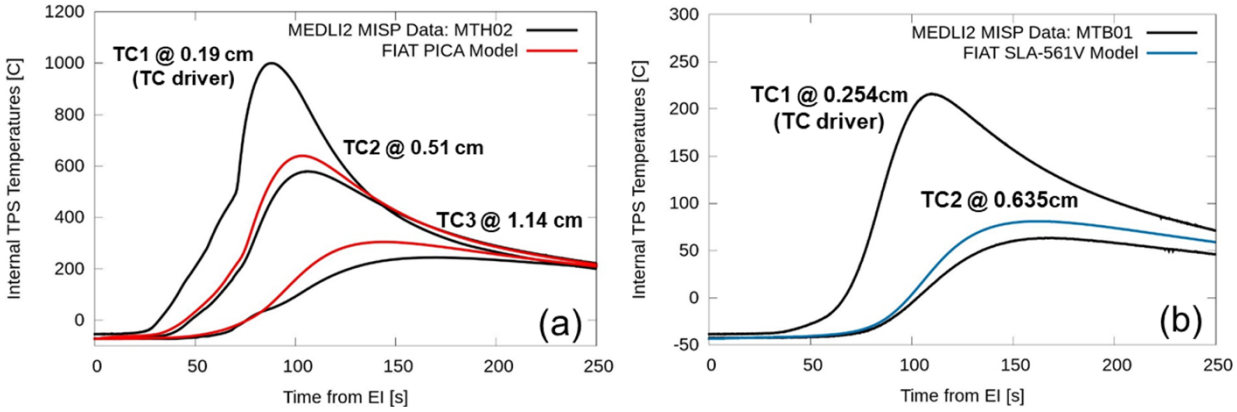


**Fig. 29 MEDLI2 measured temperature data for a) PICA heatshield TC plug b) SLA-561V backshell TC plug are compared to FIAT TC1 driver 1D material response predictions using Mars 2020 TPS sizing analysis material models**

## VII. Conclusion

The analysis methodology and results presented in this paper demonstrate that the design thickness of TPS materials on Mars 2020 aeroshell were sufficient to shield the underlying structure from the predicted entry heating environments. Key differences from MSL analysis included the addition of shock-layer radiation in heating environments, identification of bounding trajectories for each TPS sizing location from two separate dispersed Monte Carlo sets, and a more extensive analysis of PCC/BIP hardware elements (required mainly due to the change in heating distribution/magnitude after the inclusion of radiative heating). Heatshield sizing was performed at the peak heating location assuming the maximum initial temperature and the lightest structure in the heatshield. The PICA design thickness had significant margin even with the conservative analysis process employed here. Backshell sizing was done at two locations considering the varying aerothermal environments and initial temperatures. The lightest structure material stack was used in the analysis. As with the PICA, the SLA-561V design thickness had significant margin even with conservative analysis assumptions. PCC/BIP sizing had to be performed at multiple locations with different analysis assumptions to account for the changing substructure, different bondline temperature requirements and varying aerothermal environments. A total of 17 sizing cases were considered. The Acusil-II design thickness at all the sizing locations was shown to be sufficient, having significant margin in most places.

Testing of all Mars 2020 TPS materials in the NASA Ames arc jet facilities demonstrated that the flight lot TPS materials performed as expected without any flaws or failures and consistent with prior testing. FIAT predictions were compared with test measurements to assess the accuracy of thermal response models used in TPS sizing. These simulations demonstrated that the thermal response of Mars 2020 flight-lot TPS materials were in family with their historical performance and consistent with thermal response model predictions.

Additionally, temperature data returned by MEDLI2 thermocouples that were installed in the flight TPS were compared with the thermal response model predictions. This comparison showed that the models used in TPS sizing and design overpredict the flight data, suggesting that FIAT TPS sizing analysis provided conservative sized thicknesses.

## Acknowledgments

The authors gratefully acknowledge the effort of the entire Mars 2020 aerothermal and TPS team across NASA Ames and Langley Research Centers, Jet Propulsion Laboratory, Lockheed Martin, Fiber Materials Inc. and Peraton.

## References

[1] Tran, H., Johnson, C., Rasky, D., Hui, F., Chen, Y.-K, and Hsu, M., "Phenolic Impregnated Carbon Ablators (PICA) for Discovery Class Mission," *31st AIAA Thermophysics Conference*, AIAA 96-1911, New Orleans, LA., June 1996.

[2] Willcockson, W.H., "Stardust Sample Return Capsule Design Experience," *Journal of Spacecraft and Rockets*, Vol. 36, No. 3, 1999, pp. 470-474.

[3] Beck, R., Driver, D., Wright, M., Laub, B., Slimko, E., Edquist K., Thames, T., Willcockson, W., Sepka, S., and Hwang, H., "Development of the Mars Science Laboratory Heatshield Thermal Protection System," *Journal of Spacecraft and Rockets*, Vol. 51, No. 4, 2014, pp. 1139-1150.

[4] Szalai, C., Slimko, E., Hoffman, P., "Mars Science Laboratory Heatshield Development, Implementation, and Lessons Learned," *Journal of Spacecraft and Rockets*, Vol. 51, No. 4, 2014, pp. 1167-1173.

[5] Laub, B., Chen, Y., and Dec, J., "Development of a High-Fidelity Thermal/Ablation Response Model for SLA-561V," *41st AIAA Thermophysics Conference*, AIAA 2009-4232, San Antonio, Texas, June 2009.

[6] Wright, M., Beck, R., Edquist, K., Driver, D., Sepka, S., Slimko, S., and Willcockson, W., "Sizing and Margins Assessment of Mars Science Laboratory Aeroshell Thermal Protection System," *Journal of Spacecraft and Rockets*, Vol. 51, No. 4, 2014, pp. 1125-1138.

[7] Edquist, K. T., Dyakonov, A. A., Wright, M. J., Tang, C. Y., "Mars Science Laboratory Entry Capsule Aerothermodynamics Environments," JPL Document D-34661, November 2010.

[8] Edquist, K.T., Dyakonov, A.A., Wright, M.J., and Tang, C.Y., "Aerothermodynamic Design of the Mars Science Laboratory Heatshield," *41st AIAA Thermophysics Conference*, AIAA 2009-4075, June 2009.

[9] Edquist, K. T., Wise, A. J., Johnston C. O., Prabhu, D. K., and Saunders, D. A., "Mars 2020 Entry Capsule Aerothermal Environments," JPL Document D-101339, April 2020.

[10] Mazaheri, A., Gnoffo, P. A., Johnston, C. O., and Kleb, B., "LAURA User's Manual: 5.5-65135," NASA TM 2013-217800, NASA Langley Research Center, February 2013.

[11] Wright, M. J., Candler, G. V., and Bose, D., "Data-Parallel Line Relaxation Method for the Navier-Stokes Equations," *AIAA Journal*, Vol. 36, No. 9, 1998, pp. 1603-1609.

[12] Brandis, A., White, T., Saunders, D., Hill, J., Johnston, C., "Simulation of the Schiaparelli Entry and Comparison to Aerosciences Flight Data," *Journal of Spacecraft and Rockets*, Vol. 59, No. 9, 2021, pp. 166-177.

[13] Johnston, C. O., Brandis, A. M., and Sutton, K., "Shock Layer Radiation Modeling and Uncertainty for Mars Entry," *43rd AIAA Thermophysics Conference,* AIAA 2012-2866, New Orleans, LA, June 2012.

[14] Cruden, B. and Brandis, A. M., "Updates to the NEQAIR Radiation Solver," Tech. Rep. ARC-E-DAA-TN19271, NASA Ames Research Center, November 2014.

[15] Chen, Y. and Milos, F., "Ablation and Thermal Response Program for Spacecraft Heatshield Analysis," *Journal of Spacecraft and Rockets*, Vol. 36, No. 3, 1999, pp. 475-483.

[16] Milos, F. and Chen, Y., "Ablation, Thermal Response, and Chemistry Program for Analysis of Thermal Protection Systems," *Journal of Spacecraft and Rockets*, Vol. 50, No. 1, 2013, pp. 137-149.

[17] Milos, F. and Chen, Y., "Ablation and Thermal Response Property Model Validation for Phenolic Impregnated Carbon Ablator," *Journal of Spacecraft and Rockets*, Vol. 47, No. 5, 2010, pp. 786-805.

[18] Beck, R., "Thermal Characterization and Modelling of Hera Reentry Vehicle Thermal Protection System Materials," Reference No. 724A-93-0247, Aerotherm Corporation, Mountain View, California, November 1993.

[19] "MSLA Aeroshell Structure Thermal Properties: For Use in TPS Response Analysis," Lockheed Martin Space Systems Report, April 9, 2008.

[20] Sepka, S. and Wright, M., "A Monte Carlo Approach to FIAT Uncertainties - Improvements and Applications for MSL," *41st AIAA Thermophysics Conference*, AIAA 2009-4243, San Antonio, Texas, June 2009.

[21] Bose, D., White, T., Mahzari, M., "Reconstruction of Aerothermal Environment and Heat Shield Response of Mars Science Laboratory," *Journal of Spacecraft and Rockets*, Vol. 51, No. 4, 2014, pp. 1174-1184.

[22] Driver, D., Carballo, E., Beck, R., Prabhu, D., Santos, J., Cassell, A., Skokova, K., Tang, C., Hwang, H., Slimko, E., Wilcockson, W., Songer, J., "Arcjet Testing in Shear Environment for Mars Science Laboratory Thermal Protection System," *Journal of Spacecraft and Rockets*, Vol. 51, No. 4, 2014, pp. 1151-1166.

[23] Szalai, C., "Acusil-II Flight Lot Verification Test Report", JPL Document D-69958, July 2011.

[24] White, T., Mahzari, M., Miller, R., Tang, C., Monk, J., Santos, J., Karlgaard, C., Alpert, H., Wright, H., Kuhl, C., "Mars Entry Instrumentation Flight Data and Mars 2020 Entry Environments," *AIAA SciTech Forum*, AIAA 2022-0011, San Diego, CA, January 2022.

[25] Monk, J., Feldman, J., Mahzari, M., Santos, J., White, T., Prabhu, D., Alpert, H., "MEDLI2 Material Response Model Development and Validation," *AIAA SciTech Forum*, AIAA 2022-0549, San Diego, CA, January 2022.

[26] Alpert, H., Saunders, D., Mahzari, M., Monk, J., White, T., "Inverse Estimation of Mars 2020 Entry Aeroheating Environments Using MEDLI2 Flight Data," *AIAA SciTech Forum*, AIAA 2022-0550, San Diego, CA, January 2022.